UNIVERSITY OF CALIFORNIA

RIVERSIDE

Strain-Based Characterization in Severe Plastic Deformation Processing

A Dissertation submitted in partial satisfaction
of the requirements for the degree of

Doctor of Philosophy

in

Mechanical Engineering

by

Evander Harrison Ramos

December 2021

Dissertation Committee:

Dr. Suveen Mathaudhu, Chairperson
Dr. Reza Abbaschian
Dr. Alex Greaney

The Dissertation of Evander Harrison Ramos is approved:

Committee Chairperson

University of California, Riverside

Acknowledgements

First, I am extremely grateful to have had Professor Suveen Mathaudhu as my research advisor. Between our aligned interests in metallurgy, superheroes, and hip hop, I could not imagine a more ideal mentor for my graduate schooling. Throughout these past few years, he has always served as an exceptional role model and source of support and encouragement, and I aspire towards a career in research as prolific as his.

I would also like to thank my dissertation committee: Professor Reza Abbaschian and Professor Peter Alexander Greaney. Having used Prof. Abbaschian's textbook in my undergraduate education (like most other materials scientists), it was surreal to go on to TA for his failure analysis class and to have his invaluable expertise in completing my dissertation. I have also been grateful to benefit from the tremendous intellect of Prof. Greaney who has always offered such stimulating questions and conversation, and I am looking forward toward successful collaboration on our antibacterial project.

My graduate studies have been funded in part by a GAANN award to UC Riverside from the U.S. Department of Education, for which I am very appreciative. I also thank the staff at UC Riverside that worked behind the scenes to take care of all the paperwork and disbursements and whatnot that goes into making graduate school run smoothly.

On the research side of things, I am indebted to our collaborators Professor Zenji Horita, Takahiro Masuda, and Yoichi Takizawa for processing the samples in our works. I am humbled by their generosity throughout our collaboration and wish for much more to come. I am grateful to have had access to the excellent facilities for microscopy and

characterization available at UCR. I will always cherish those long marathon sessions spent toiling away at the four-point probe or FIB. Additionally, I would like to thank all my cohort in the Mathaudhu lab for their support throughout the years. Between grad meetings, conferences, stress relief fairs, and fake middle names, we have always found ways to have a good time. I thank all the students from the classes I TAed who helped me improve as a teacher, especially Sarah who also helped me with some lab work.

I would also like to thank the team at NanoAl, including Dr. Nhon Vo, Professor David Dunand, and Professor David Seidman, for giving me my first job after undergrad and thus an entrée into metallurgy. They played a pivotal role behind the origins of this dissertation, as they pointed me toward the work of Prof. Mathaudhu and helped me with my graduate school applications, so I cannot thank them enough.

It is important to note that this work could not have been accomplished without the outstanding public transportation services provided by the Riverside Transit Agency, the Los Angeles County Metropolitan Transportation Authority, and the Metrolink. I also wish to thank my trusty steed TCHONDA, which came through at times when the bus and train would not. In addition to transportation, TCHONDA served as a valuable place to collect my thoughts, practice presentations, and consume stress induced fast food binges. Additionally, I would like to acknowledge the support of all the various forms of media I have consumed that helped me endure my long commute as well as the long hours spent in the lab. Between all the music, movies, television shows, stand-up comedy, and podcasts, it is a wonderful privilege to share and experience the talents and creativity of others.

On the personal side of things, I have always been grateful for the support of my family. Many thanks to my partner and best friend Janay for her constant support and encouragement and for the fact that if she could be any keyboard key she would be F12. I still remember that cake she got me after I was accepted to UCR that had “Dr.” in front of my name; it turns out that cake was not a lie. We finally made it through these hectic few years of finishing up our education, and who knows, we might even rule the world one day. Thanks to Jess’Ca for being the goodest girl, for occasionally accompanying me on my travels to help make the commute more bearable, and for always being a spirit of coziness by which we could enjoy some relaxation vicariously. To all my family back at home in Chicago, I am thankful for all the love and support from afar. I owe so much of my values to you all, so this dissertation is truly a success for all of us. To my in-laws in North Carolina and Atlanta, we are grateful for all of your generosity and support, from TCHONDA, to words of encouragement, and care packages of spices. Additional thanks go out to all my friends who have helped me hone my skill at describing my research in the most crude and digestible ways possible.

While an “acknowledgements” section is typically intended for giving thanks and expressing gratitude, I feel I would be remiss to not also acknowledge the chaotic times in which this dissertation was completed. This work was carried out amidst a global pandemic, a nationwide reckoning with racial injustice, and a growing public mistrust and misunderstanding of science. With the disastrous effects of climate change also becoming more apparent every year, it is imperative to reverse the tides of our societal misperceptions and work together toward a greater future than the one to which we are

currently headed. Two of the concepts that have guided my life over the past few years have been the ideas of "lighting your corner" and "spending your privilege." I sincerely hope that my graduate education affords me the privilege to expand my corner to help create a better tomorrow.

Lastly, I would like to thank Toni Morrison for a lifetime of brilliant and inspirational work, especially the following quote which has been on my conscience throughout my graduate studies:

"We die, that may be the meaning of life. But we do language. That may be the measure of our lives."

To Nestor and Enemina, thank you for everything

ABSTRACT OF THE DISSERTATION

Strain-Based Characterization in Severe Plastic Deformation Processing

by

Evander Harrison Ramos

Doctor of Philosophy, Graduate Program in Mechanical Engineering
University of California, Riverside, December 2021
Dr. Suveen Mathaudhu, Chairperson

Scientific innovation is often driven by novel processing capabilities, which enable the production of materials with new and exciting properties. Several techniques referred to as severe plastic deformation (SPD) have recently been established, which utilize extreme strain conditions to create advanced materials. Such processing has the potential to provide materials solutions to current technological issues humanity faces in areas such as energy, transportation, sustainability, and public health. Additionally, these processes enable exploration of complex microstructures to better understand fundamental relationships between processing, structure, properties, and performance.

The SPD literature consists of many studies reporting the structures and properties garnered from a wide variety of techniques, material systems, and processing conditions. In some cases, reports may be at odds with each other or with expected material behavior, as has been the case for wear resistance and electrical conductivity. For both properties,

strain-based characterization can improve comparison across the literature to better understand trends and highlight outlier reports in the established literature. For some processes, strain-based investigations may not even be reported, so novel characterization or analysis methods are necessary to enable such comparison across the SPD literature.

In this dissertation, results from experiments on copper subjected to SPD processing has been compared to reports from the literature to identify trends in wear resistance and electrical conductivity across SPD techniques. To accomplish this, novel strain-based analysis and measurement methods have been put forth for the process of high-pressure torsion. These frameworks of strain-based analysis enabled trends to be drawn from comparison with the SPD literature, which has also helped to distinguish outlying existing reports and forecast results of previously untested processes. Additionally, the newly enabled strain-based characterization has indicated some trends for SPD wear resistance in relation to strain orientation which had previously gone undetected despite corroborating evidence being scattered across multiple prior reports. To explore this relationship between wear path and strain path, the properties of copper subjected to high-pressure sliding has been explored at different strains and orientations. General microstructural behavior was found to agree with the greater SPD literature as well as the identified strain path dependence indicating that lower wear rates are seen when wear is conducted parallel to the shearing direction. Future works can adapt the comparative analytical frameworks demonstrated in these studies to identify strain-based relationships for other properties, such as magnetism or antibacterial resistance, to inform the development of advanced materials.

Contents

List of Figures

List of Table

Introduction

The central paradigm driving materials development throughout the history of mankind is the relationship between processing, structure, properties, and performance. Improved understanding of the relationship between these four components has unlocked numerous technological advances throughout the years. With advancement in processing technologies, opportunities to explore and better understand this paradigm are unlocked. Within the past few decades, the development of severe plastic deformation (SPD) processing techniques has enabled the creation of unprecedented materials and opened many avenues for scientific exploration [1]. SPD techniques are marked by their ability to impart large strains into worked samples while generally maintaining their original dimensions. This contrasts with conventional processing techniques such as rolling, forging, or drawing where dimensions are reduced by mechanical straining. Unlike these conventional processing techniques, SPD processes have the potential to quickly create ultrafine grained (UFG) (average grain size between 100 and 1000 nm) or even nanocrystalline (NC) (<100 nm) microstructures [2]. These microstructures can have unique properties with significant improvements compared to their conventional coarse-grained counterparts. While other processes, like thin film deposition techniques, can create similar microstructures with extremely small grain sizes, the ability of SPD to produce them in large volumes is ideal for exploration of processing-structure-properties-performance relationships.

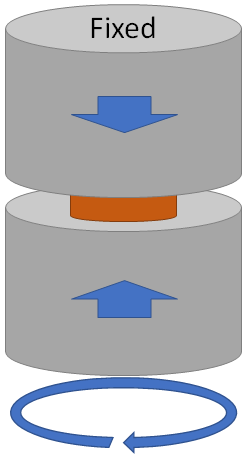

Figure 1: Schematic representation of the method of high-pressure torsion for processing a sample (orange) between two anvils (grey).

Of the many SPD processing techniques that have been developed, one that has attracted significant research interest is high-pressure torsion (HPT). In HPT, material is compressed at high pressures between two anvils, and thereafter one anvil is rotated to impart significant torsional shearing, as shown schematically in Figure 1.1. Samples are commonly small discs, measuring around 10 mm in diameter and 1 mm thick, although a wide variety of sample dimensions have been explored. Some examples of unconventional sample dimensions include rings [3], thick cylinders [4], or rods via continuous HPT [5]. The deformation under high pressures has been reported to drive phase transformations that remain stable after processing is complete [6]. HPT can even create composites and mechanically mix different metals [7]. A wide variety of interesting materials can be made from HPT, which is why characterizing their properties has been an area of active research. HPT processing has the potential to provide transformative material solutions to advance technologies in areas such as energy, transportation, health, and many others.

One issue with HPT is the relatively small samples it can process, which makes it unattractive for scalable manufacturing. Significant efforts have been advanced to modify HPT or use alternative deformation schemes at high pressures [8]. One such recent development is high-pressure sliding (HPS). This technique is essentially a linear version of HPT, where in lieu of rotational torsion, a sample is sheared uniformly by planar sliding. This process is more scalable and has been demonstrated to process large volumes of 50 x 100 x 1 mm^3 sheets [8]. Despite the ease of implementing large strains and the potential for scalability, HPS is still in its infancy and much work needs to be done to validate the structures and properties it creates in reference to the other SPD processes.

To provide a broader scope of high strain processing, a few of the other SPD processes will be highlighted. Alongside HPT, the other technique that has received the most attention and exploration is equal channel angular extrusion (ECAE). Also referred to as equal channel angular pressing, ECAE involves pressing a billet through an angled channel. Traversing through the angled portion of the channel imparts large strain into the billet without significantly altering the dimensions. With low pressures and low strain accumulation per pass, this process is typically repeated multiple times to achieve highly strained samples. Similar to HPS, this technique imparts strain uniformly throughout the processed material, but the strain path can be varied by rotating the sample between iterations. Similar to HPT, significant efforts have been put forth to scale this process up to industrial manufacturing [9]. Alternatively, instead of processing entire volumes of materials, some SPD techniques are confined to the surface, such as in surface mechanical attrition treatment (SMAT). In SMAT, hard balls repeatedly strike a surface to induce

significant microstructural refinement in the near surface region. Similar to HPT, this process results in a gradient in strain throughout the processed sample. The highest strain is found at the surface, and it rapidly deteriorates as a function of depth. Lastly, although mechanical alloying is not technically considered an SPD process due to significant changes in the sample dimensions, it is able to create similar microstructures by extreme shearing. Powders are sealed in a jar and subjected to vigorous ball milling. The repeated high-energy impacts alter the powder by either breaking particles down or welding them back together. Altogether, the result is a stochastic process which can yield powders with nanostructured or nonequilibrium microstructures, albeit with potentially high levels of impurities picked up from various sources. These powders can then be consolidated via powder metallurgy, with additive manufacturing specifically being an area of active research.

To compare between SPD processes, there has been extensive efforts to calculate idealized equivalent strains for a given process [10]. Formulae have been developed to describe the equivalent strain that an idealized grain will endure due to SPD. As these equations are idealized, they often neglect things like material slipping, deformation from the initial loading force (as in HPT), or heat evolution from straining. Nevertheless, they provide a useful and generally accurate way to compare between processes. Among SPD processes, HPT is most readily able to achieve high strains with minimal processing of only a few rotations. This strain is also inhomogeneous, with strain increasing linearly as a function of the radial distance from a theoretically strain-free center.

Structure evolution with strain has been well documented for various SPD processes [2]. SPD processes essentially impart massive amounts of dislocations into processed materials. These interact and end up forming dislocation cells and sub-grains which eventually reorganize into well-defined grain boundaries. Further straining of these small grains can result in dynamic recrystallization, resulting in larger grains which can then undergo the process again to be refined back into small grains. Therefore, materials can approach an equilibrium grain size when there is a balance between grain refinement and dynamic recrystallization from further straining. It should be noted that this description of grain refinement in SPD is a generalization, as materials pass through the different stages at different rates based on intrinsic material characteristics such as stacking fault energy. Researchers often look for ways to exploit and manipulate the structure evolution in SPD to improve performance, such as by annealing or judicious alloying additions. Understanding how properties evolve as these structures are developed based on the imposed straining is key toward taking advantage of these techniques for producing useful engineering materials. For certain properties, there is good understanding of these relationships, such as the Hall-Petch effect for hardness [11].

There are gaps in SPD literature reflecting a lack of understanding how certain properties vary with processing strain. Many works have been devoted to assessing the properties of materials subjected to various SPD processing conditions. Typically, microhardness is tested to give an indication of strength and other properties, but actual measurements of these other properties may at times not follow trends with hardness as expected. For wear resistance, one review article has noted inconsistent trends where some SPD processes are

beneficial while others are not, with some processes even having conflicting reports on their improvement [12]. Other properties, such as antibacterial resistance, have not been described by SPD review articles, although a few articles on different processes have reported improvements [13], [14].

To understand how properties vary with processing strain, researchers must make a concerted effort toward strain-based characterization. Specifically for HPT, the inhomogeneity imparted by the process is often overlooked when characterizing certain properties. Many HPT works have characterized inhomogeneity by analyzing the microstructures that are formed in different locations throughout processed samples or by taking hardness indentations at various locations. Since such characterization can be applied locally at small, well-defined positions, it is easy to calculate the equivalent strain for the region of interest and thereby microstructural and hardness evolution with strain is accomplished. However, many other characterization techniques require larger areas or volumes of material to be conducted.

For example, wear is commonly tested by sliding tests across sample surfaces. Wear tests can leave a large footprint, below which a large interaction volume contributes toward the measured wear response. A representation of the impact this has on wear testing of HPT materials can be seen in Figure 1.2. Although shorter wear tracks could be used to cover smaller range of strains, changes in testing procedures alters the wear modes that are being activated, and thus limits their practicality and utility. As noted in the previous review paper on conflicting SPD wear results, wear is a complex phenomenon and there is currently only a loose understanding of its dependence on many different factors [12].

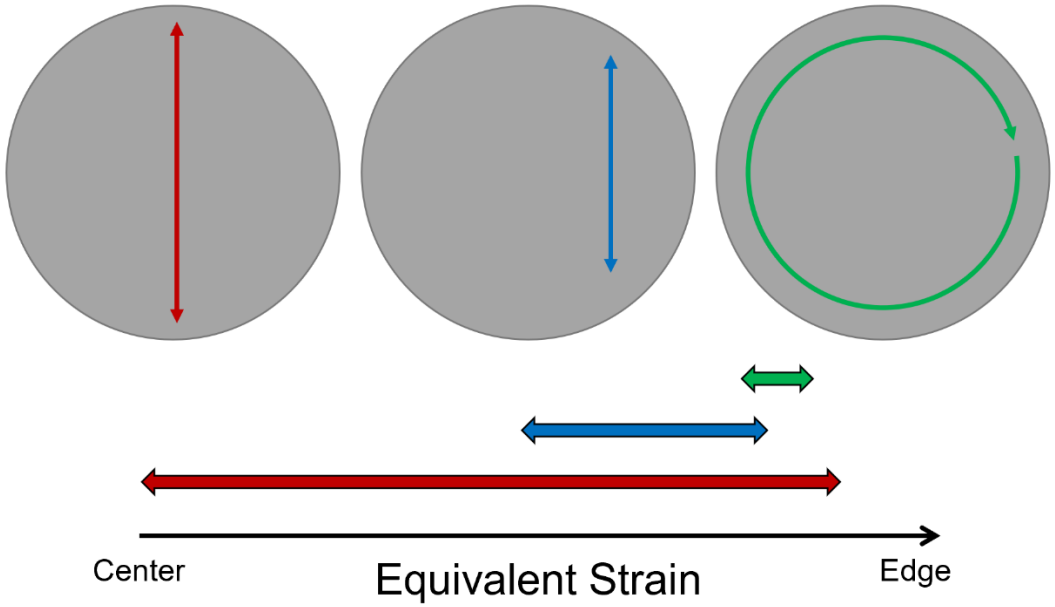

Figure 2: Schematic illustration demonstrating the ranges of strains that are covered by conducting wear tests in three different locations on an HPT disc.

For electrical conductivity, measurements are typically taken by stimulating an electrical response in a certain interaction volume. For various types of tests, this interaction volume may be a section cut from the sample or even the entire sample itself. Calculation of electrical properties from measurements is dependent on the dimensions of the interaction volume, so tests across smaller volumes (i.e. shorter ranges of strains in HPT processed materials) are prone to higher error. Conductivity evolution with strain for HPT processed materials has largely been inefficiently conducted by processing many samples and sectioning them so individual samples reflect individual data points. An improved method for conductivity characterization with strain in HPT materials can more efficiently probe variations to better understand processing-structure-property relationships.

With increased ability to characterize variations in properties with processing strain in HPT materials, the ability to correlate such variations between other SPD processes at similar strains is enabled. Aside from hardness, a comprehensive understanding of property evolution as a function of strain irrespective of the specific process used is currently lacking for many properties. A better understanding of how properties such as wear resistance and electrical conductivity vary with strain in HPT materials can be compared to the wider SPD literature to assess trends.

From an applications perspective, it is also imperative to understand the dependence of wear on strain to forecast resiliency. If SPD materials are to be used in the future, scientists and engineers should be able to estimate things like their wear properties based on processing. Improved understanding of these relationships can speed up materials development and assist in pinpointing what processing strains to target for a desired performance. On a broader level, wear itself is also a large strain process which can potentially impart significant microstructural refinement near the surface. Since wear is a process that can also create UFG structures, a better understanding of the evolution of wear behavior in UFG materials processed by SPD can be useful for understanding wear in all materials.

To summarize, this dissertation will address knowledge gaps in property variation with strain in SPD copper. By using novel testing procedures and analysis, relationships between equivalent strain and wear resistance and conductivity are measured throughout HPT discs. These novel measurements enable comparison across SPD processes to develop a more comprehensive understanding of strain-based property relationships irrespective of

the specific processing method. Additionally, such testing will also be conducted on HPS processed copper to validate postulated overarching strain-based property relationships. Supplemented with the vast literature for SPD processes, the HPT and HPS results contribute toward a better mechanistic understanding of the directional dependence of wear in relation to shear processing.

Chapter 1

Strain effects on the wear rate of severely deformed copper

Evander Ramos[a], Takahiro Masuda[b], Sina Shahrezaei[c], Zenji Horita[b], Suveen Mathaudhu[ac]*

[a] Department of Mechanical Engineering, University of California, Riverside, United States

[b] Department of Materials Science and Engineering, Kyushu University, Fukuoka 819-0395, Japan

[c] Department of Materials Science and Engineering, University of California, Riverside, United States

* Corresponding author: smathaudhu@engr.ucr.edu, Bourns Hall A325, 900 University Ave., Riverside, CA 92521

Abstract

A variety of severe plastic deformation (SPD) techniques have been developed to process materials to high strains and impart microstructural refinement. High pressure torsion (HPT) is one technique that imparts inhomogeneous strain to process discs with low strain in the center and high strain at the outer edge. In the literature, this inhomogeneity is typically ignored when characterizing wear properties after HPT. In this work, the wear

rate of pure copper discs processed by HPT was characterized by conducting dry sliding reciprocating wear tests at a few judicious locations on the discs. From only two discs, the wear resistance across many ranges of strains was captured. These measurements agreed with the literature for other SPD processes at varying strains. Wear rates dropped and plateaued at about 25% that of the unprocessed state when processing past equivalent strains of around 15, after which microstructural and microhardness saturation has also been observed. Some indication of a relationship between the direction of the imposed SPD shearing and the sliding wear direction was also observed. The incremental microstructure, microhardness, and wear resistance evolution past equivalent strains of ~15 indicate that for high purity copper these properties receive no clear benefit from higher SPD strains.

Keywords: Sliding wear, ultrafine-grained, copper, high-pressure torsion, severe plastic deformation, equivalent strain

1. Introduction

Severe plastic deformation (SPD) techniques have been well-documented for processing materials to obtain ultrafine-grained (UFG) or nanograined microstructures [15]. Among SPD processes, high-pressure torsion (HPT) is attractive because the microstructural refinement it imparts is quick and efficient although also inhomogeneous throughout the disc at low equivalent strains (i.e. number of turns) [15]. This inhomogeneity varies due to the amount of imposed equivalent strain (ε) throughout the disc during processing, which

is commonly calculated from equation (1), where r = radial distance, N = number of rotations, and t = thickness [15].

$$\varepsilon = \frac{2\pi r N}{\sqrt{3}\, t} \qquad (1)$$

In the literature, hardness measurements are commonly used to indicate the degree of microstructural homogeneity throughout HPT discs [16]. However, other properties such as wear rate or friction can also vary with the equivalent strain, and they may do so in ways that do not follow the same trends indicated by hardness variations throughout discs.

Inhomogeneity is often ignored in reports of the wear response of HPT materials. Continuous ball-on-disc wear testing (ASTM G99) has been used [17]–[20], but these tests only cover localized and distinct levels of equivalent strain (i.e. sliding along one specific radial distance), and do not characterize the wear behavior in other regions across the diameter of the discs. Other studies [21]–[30] have used linear reciprocating ball-on-flat wear tests (ASTM G133) which cover a wider range of strain regimes and microstructures. But, these reciprocating wear tests are typically conducted at only one location without comparing to other locations on the discs. Thus, reported wear rates for HPT materials have been generalizations based on tests of one section of a disc. Furthermore, a review article on the wear performance of SPD-processed UFG materials has highlighted conflicting reports of both improvements and reductions in wear rates observed after HPT for different material systems, a phenomenon that was also seen in some materials after equal channel

angular extrusion (ECAE) [12]. This article hypothesized that in some cases the wear resistance increased due to the smaller grains and higher hardness from SPD, whereas in other cases the wear resistance decreased due to reduction in ductility and strain hardening capability after SPD processing. It is also possible that the specific regions of equivalent strain covered by the wear tests can influence the resulting wear response measured, and so experiments analyzing different locations of processed samples can be contributing to these conflicting reports. Thus, the accuracy of wear response characterization in HPT materials can be improved by accounting for the variation in equivalent strain throughout discs, facilitating observations of correlations between these properties and the microstructures produced.

To probe wear properties with respect to the equivalent strain from HPT processing, linear reciprocating wear tests were conducted at judicious locations covering different ranges of strains. These results were compared to the literature to observe trends with equivalent strain across various processing methods. Pure copper was chosen as the material system due to the wealth of SPD literature accumulated for comparison, along with its relevance for commercial applications. The present work reports that wear rate follows trends in microstructural and microhardness evolution with processing strain, but also a relationship between wear path and strain path has been observed.

2. Materials and Methods

High purity copper (99.99 wt%) with an initial grain size of ~20 μm was sliced into discs 10 mm in diameter and 1 mm thick before being annealed at 873K for 1 hour. These discs were subjected to HPT in air and at room temperature at a pressure of 6 GPa for 1 and 10 rotations. After HPT, the flashing was removed, and surfaces were ground flat up to 1200 grit. The discs were kept in air at room temperature for about 2 years before characterization. To prepare the surfaces for characterization, the discs were electropolished at 4.7 V for 90 s in a 200 mL solution of 10:5:5:1 H_20:phosphate:ethanol:IPA with 1 g urea [31]. Immediately afterwards, the discs were rinsed thoroughly in deionized water followed by IPA. Vickers microhardness was measured with a Phase II Vickers Microhardness Indenter with a 200 g load and 15 s dwell time. Indentations were taken along four diameters and spaced 0.5 mm apart. Microstructural characterization was carried out using an FEI Nano NovaSEM 450 scanning electron microscope (SEM) with a concentric backscatter detector (CBS). Average grain size was determined using Abrams three-circle procedure. A foil was extracted from the half radius of the 10 rotation sample using an FEI Quanta™ 3D 200i focused ion beam (FIB). This foil was used for transmission electron microscopy (TEM) using a Titan Themis 300 at 300kV.

Unlubricated linear reciprocating ball-on-flat wear tests were conducted on full uncut discs using a Nanovea mechanical tester in accordance with ASTM G133. A normal force of 5 N was applied for a stroke length of 3 mm at a frequency of 0.25 s^{-1} for a total sliding

distance of 10 m and a total time of under 2 hours. Tests were conducted in air at a relative humidity of 44±2% and at room temperature (22±1.5°C) for all samples. The wear test parameters used in this study were chosen to ensure mild sliding and to be similar to other wear studies on pure copper to facilitate comparison. Mild sliding was achieved by using slow sliding speed to avoid excessive frictional heating and a low load with hard and tough wear balls to limit external transfer onto the copper surface. A new 3 mm diameter ball of 6% Co-cemented WC was used for each track and inspection determined that negligible ball wear occurred with little adherence of wear debris. These sliding parameters help to isolate the mechanical deformation of the ultrafine grained copper microstructure during wear. A foil from the center of the high strain tangential wear track on the 10 rotation disc was extracted using FIB lift-out technique and imaged using a Tecnai12 TEM at 150kV. This wear track was chosen for an initial exploration of the subsurface microstructural evolution due to it having been deformed to the highest strain level.

On each disc, wear tests were carried out at four locations, one of which spanned along the radius between 1 and 4 mm away from the center (herein called “radial tests”). The other three tests were centered at various distances from the center such that they would be parallel to the tangent of the disc (herein called “tangential tests”). The test locations were deliberately chosen so the tangential tests were near the highest, lowest, and average equivalent strain regions of the radial tests. In other words, the tangential tests covered small ranges of strains corresponding to those encountered at the center and either end of the radial test. Only one test was conducted at each range of strains, so no standard

deviations could be provided for the HPT processed disc tests. This is in part due to dimensional limitations of the processed discs, which may be a contributing factor into why such tests have not been conducted on HPT discs in the literature. The resulting wear tracks were cleaned with compressed air and evaluated using a Nanovea optical profilometer and analysis software to determine the profile of the scar with 10 μm resolution parallel to the track and 1 μm resolution perpendicular to the track. Specific wear rate was calculated by dividing the measured wear volume at the conclusion of the test by the total sliding distance and load.

3. Results

3.1. Typical microstructures after HPT

As in prior works on HPT Cu, the microstructures varied radially throughout the processed discs [32]–[36]. Micrographs of the characteristic microstructures near the center and edge of discs after 1 and 10 rotations of HPT are shown in Figure 2.1. In the 1 rotation sample (Figure 2.1A), the grain sizes were heterogeneously distributed with a bimodal combination of large grains and small sections of highly refined grains. The center of the disc had the largest average grain size, while the outer edge had more regions of highly refined grains. From the SEM images taken at various locations throughout the disc, the overall average grain size was 700 nm ± 200nm. Conversely, the 10 rotation sample had mostly highly-refined grains with some large grains scattered throughout the disc, giving an average grain size of 290 nm ± 150nm. These large grains were most prevalent near the center and gradually became scarcer toward the edges.

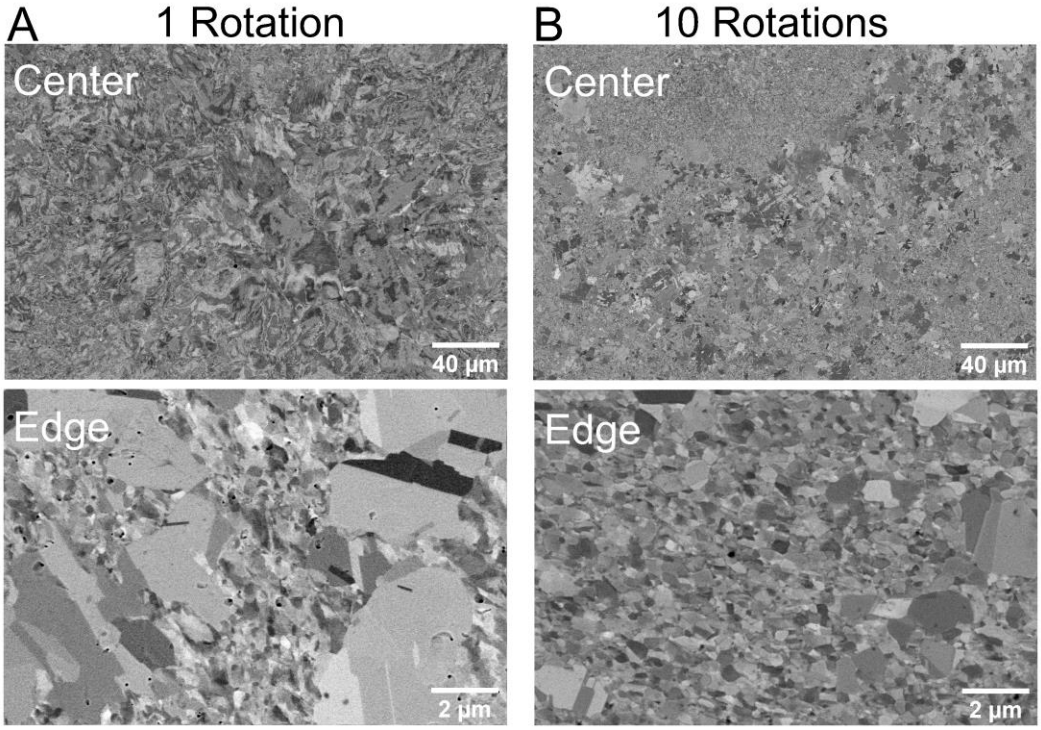

Figure 3: Micrographs displaying representative microstructures near the center and the edge of copper processed by HPT after 1 (A) and 10 (B) rotations.

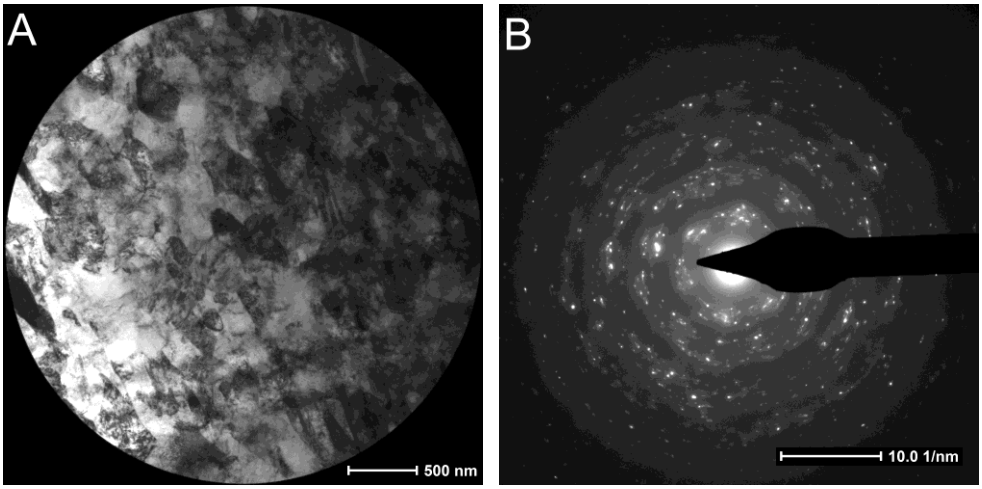

Figure 4: Transmission electron micrograph of a foil taken from the half radius of the 10 rotation sample (A) and the accompanying SAED pattern for this location (B).

The microstructure at the mid-radius of the 10 rotation sample seen using TEM is shown in Figure 2.2A, further validating the previous observations from SEM. The SAED pattern of this location shown in Figure 2.2B exhibits a diffuse ring pattern, indicating the presence of many different grain orientations as well as a high degree of lattice strain. The average grain size of 250 nm ± 66 nm measured from TEM images agreed with the averages determined from SEM.

3.2. Microhardness inhomogeneity after 1 rotation, saturation after 10 rotations

The microhardness results for the current study are shown in Figure 2.3A. Microhardness saturated at around 130 HV for the outer section of the 10 rotation sample, with a slight decrease near the center. For the 1 rotation sample, microhardness values are highest near the center, decreasing dramatically to 80 HV at 1.5 mm from the center, after which it steadily increases with radial distance. The error bars shown represent one standard deviation but are too small to be seen behind the points themselves for most of the data. The largest error is seen in the central portion of the 1 rotation sample, where the values decreased precipitously.

3.3. Higher strain generally decreases wear rate

Wear results for the four wear tests on each disc are shown in Figure 2.3B. The inset schematic shows the locations of the reciprocating tests on the HPT discs. For the unprocessed disc, the average specific wear rate for the four tests was $7.0 \times 10^{-5} \pm 1.3 \times 10^{-5}$ $mm^3/N\text{-}m$. With only one test done for each location on the processed discs, it is difficult

to tell the statistical significance of the differences between each tested location. Nevertheless, the specific wear rates for all tested locations on the processed discs were between 2.7×10^{-5} and 1.0×10^{-5} mm^3/N-m, clearly outside the range of the unprocessed disc. Comparing the two processed discs, each test from the softer 1 rotation disc had a higher wear rate compared to the corresponding test on the harder 10 rotation disc. This is in agreement with the Archard equation, stated in equation (2), which relates wear volume V, a dimensionless constant K, normal load N, total sliding distance L, and the hardness of the contacting surface H [37].

$$V = \frac{KLN}{H} \qquad (2)$$

The Archard equation can also explain differences between the three tangential tests on each disc. For the 10 rotation disc, microhardness increases slightly with equivalent strain, and accordingly the wear rate decreases from the low to high strain tests. For the 1 rotation disc, since the low strain test partially traverses the harder central region of the disc, it has a wear rate comparable to the high strain test, with the softer middle strain section having a higher wear rate. Interestingly, the wear rate values for the tangential high strain test on the 1 rotation disc and the tangential low strain test on the 10 rotation disc are similar despite the difference in measured microhardness between the two regions (1.6×10^{-5} mm^3/N-m and 900 MPa vs. 1.7×10^{-5} mm^3/N-m and 1360 MPa, respectively). Most apparent is that the radial tests, which covered the largest ranges of strain across the discs, had higher wear rates compared to the tangential tests.

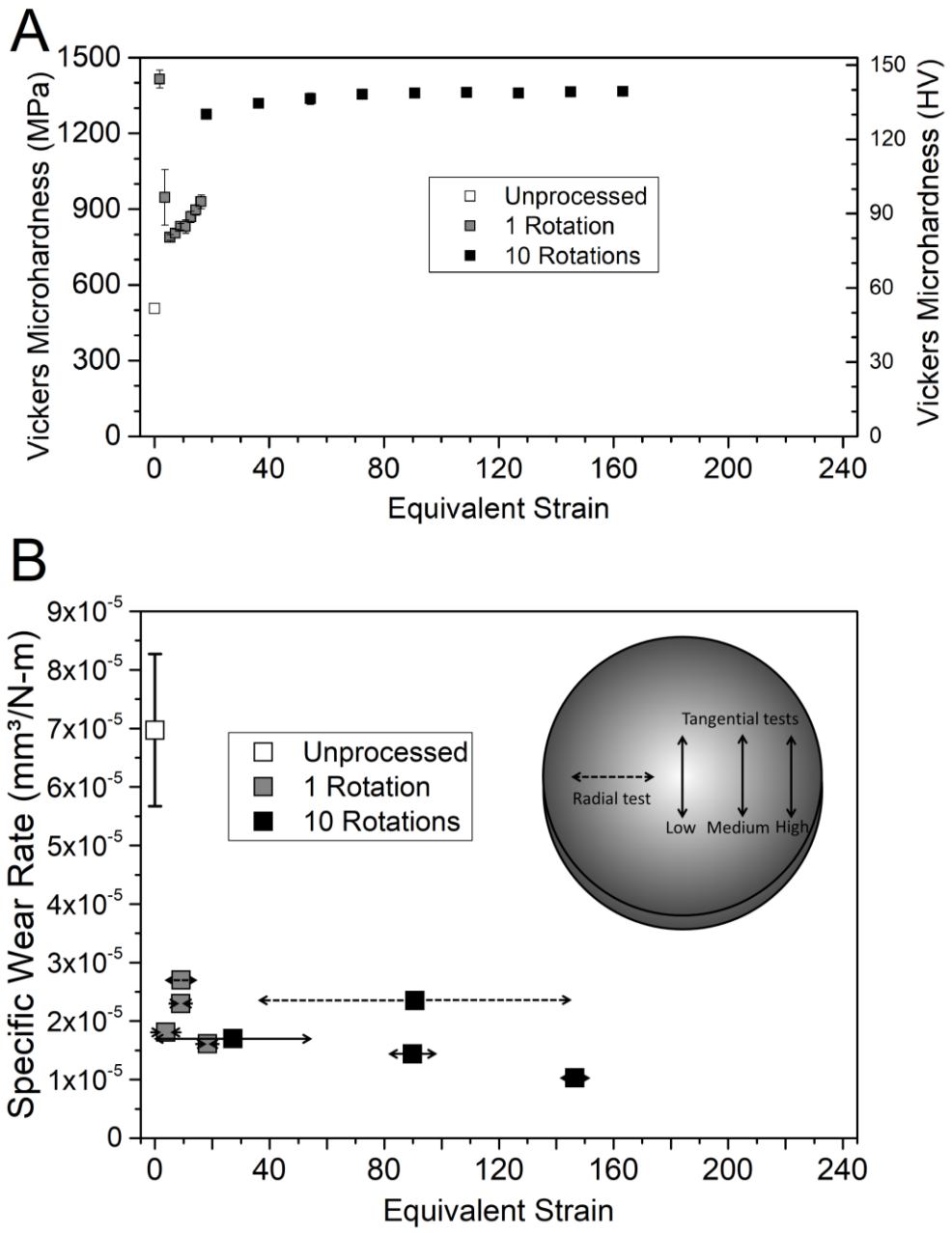

Figure 5: A) Variation in microhardness vs. equivalent strain throughout the discs after 1 and 10 rotations of HPT. B) Variation in specific wear rate vs. equivalent strain for the four tests done on each disc. The schematic inset on the right shows the locations of the reciprocating wear tests on the disc, with a gradient in color to indicate the evolution from low strain in the center (light) to high strain at the outer edge (dark). For the wear data, each data point represents the average equivalent strain along the wear track, while the x-spread represents the range of strains covered.

To compare the results from the current work to data from the literature for high purity copper processed by various SPD methods, the variation in normalized wear rate with equivalent strain was compiled as shown in Figure 2.4. Works that use various different wear test parameters can be compared via normalized wear rates, as has been previously shown for aluminum matrix composites [38]. Throughout this paper, normalized wear rate is calculated by the wear rate of the processed sample divided by the wear rate of the unprocessed control, both measured under the same conditions. Thus, a normalized wear rate of 1 indicates no change in wear due to processing, while a higher normalized wear rate indicates that the wear rate for the processed condition was higher than the unprocessed control group. A normalized wear rate less than one indicates an improvement in wear rate, e.g. a normalized wear rate of 0.5 indicates a 50% reduction in wear rate due to processing. Whenever a work used multiple wear testing parameters, the only results included are from tests with speed and load closest to the conditions used in the current work, namely 5 N load and 1.5 mm/s sliding speed.

The strain imposed by an SPD process is quantifiable by calculating equivalent strain. But, for some works in Figure 2.4, the processing imposes complex strain that is not as readily quantifiable or comparable, and those cases are simply left as bands across the equivalent strain axis. While not an SPD method, one work used electro-deposition to create samples approaching the critical grain size for the breakdown of the Hall-Petch effect [39]. Thus, it can be thought of as a limiting case for grain refinement encountered in SPD processes. The work using dynamic plastic deformation (DPD) is distinct from all the others in that it

is the only one conducted in a cryogenic environment with high strain rates of 10^3 s^{-1} [40]. The deformation strain for this process has been shown to efficiently refine grains toward the nanoscale even at small strains, and thus obfuscates direct strain comparison with the other processes included in Figure 2.4 [41]. For the works using surface mechanical grinding treatment (SMGT) [42] and surface mechanical attrition treatment (SMAT) [43], strain decreases as a function of depth from the processed surface. The wear tests in the SMAT work were performed with varying loads from 5-60 N and saw that larger loads had higher normalized wear rates due to those tests penetrating toward the larger grained, less strained regions farther below the processed surface [43]. Another work used columnar microstructural features in a steel sample to determine SMAT strain, and from an exponential fit the near surface shear strain was estimated to be around 90 [44]. Thus, the data points for such surface processing techniques can be reasonably thought of as corresponding to high equivalent strains.

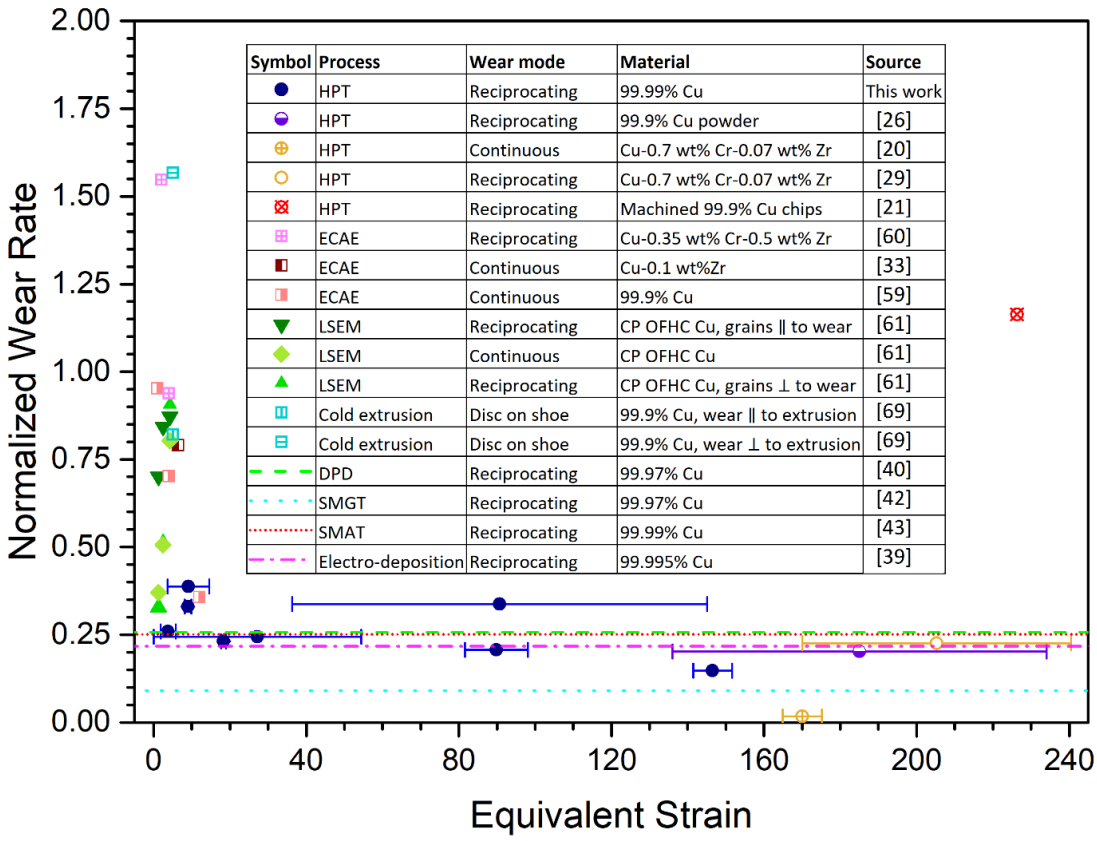

Figure 6: Normalized wear rate variation with equivalent strain for the wear tests from this work compared with other works on >99% pure copper processed by various methods. Normalized wear rate is calculated by dividing the reported wear rate or wear volume of the processed condition by the result for the unprocessed condition, thus each work is essentially normalized against itself.

3.4. Friction response and microstructural evolution below the wear track is similar to prior works

Although not the focus of the current work, frictional data was also measured continuously throughout each test. For each track, the coefficient of friction (COF) evolved rapidly, reaching an early peak after less than a few hundred centimeters of total sliding, after which it dropped slightly and thereafter slowly climbed to a steady state value for the last few

meters of the test. The average steady state COF for the four tests was 0.59 ± 0.07, 0.57 ± 0.04, and 0.52 ± 0.04 for the unprocessed, 1 rotation, and 10 rotation discs, respectively. Unlike the wear rate results, the average steady state COF measurements for the radial tests were not clearly different from the tangential tests. There was higher variance with the COFs for the unprocessed disc, probably due to these wear tracks being bumpier and less smooth. These friction values are lower than some other reported values from the works in Figure 2.4, which may be attributed to the slower speeds used for this report. Another study that also used mild reciprocating sliding parameters on copper reported similar COF values [45]. Generally, the similarities in the friction measurements for all tests indicates that all tests are dominated by the same wear mode.

The microstructure below the wear track of the high strain tangential test on the 10 rotation disc is shown in Figure 2.5. A region with a nanocrystalline (NC) microstructure extending below the wear track to a depth of ~1.5 μm can be seen in Figure 2.5A. Below this NC region, the grains have an UFG structure similar to that which was present before the wear testing. Prior studies of copper microstructures after wear have also exhibited regions of nanocrystalline grains extending to various depths below the wear surface followed by a region of UFG microstructure [46], [47]. In the current study, it is difficult to clearly differentiate between the wear affected UFG subsurface region typically formed in wear and the original UFG microstructure. The grains below the nanocrystalline region do appear slightly coarser than from before the wear testing (compare to Figure 2.2A). The nanocrystalline grains immediately below the surface are shown more clearly in Figure

2.5B. The SAED from this region shown in Figure 2.5C gives no indication that any WC from the sliding ball transferred onto the wear surface, consistent with the intended mild sliding condition and observations of the ball surface and mass after testing. A large amount of Cu_2O is seen corresponding not only to the oxidized surface of the foil, but also to the oxides formed at the surface and integrated into the mechanically mixed layer. The presence of these oxides stabilizes the nanocrystalline structure near the wear surface, helping to maintain a stable average grain size on the order of 10 nm. The d-spacing for FCC cobalt (111) is 0.205 nm, similar to the d-spacing for Cu (111) which is 0.208 nm, so there is the possibility that a small amount of the cobalt binder in the ball could have transferred into the wear surface and also contributed to stabilizing the near surface nanocrystalline region. One last notable feature of Figure 2.5A is the high contrast, slightly angled crack just above the UFG layer. It may have originated within the subsurface due to the plastic deformation of the sliding or alternatively was formed at the wear surface and absorbed in the nanocrystalline layer, although it could also just be an artifact from the FIB lift out process. Further characterization of the subsurface microstructures formed below the other wear tracks should be done in future work to investigate such potential cracking in the wear affected regions of SPD processed materials.

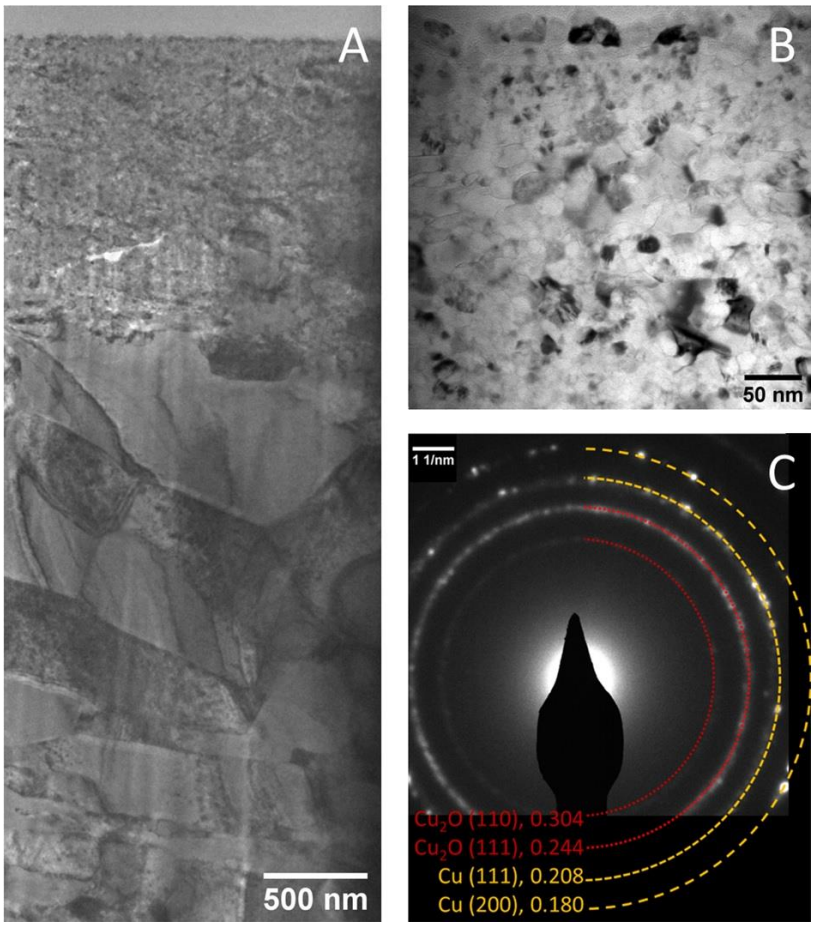

Figure 7: TEM bright field images of the grain structures formed immediately below the wear surface. A roughly 2 µm by 4 µm region below the wear surface showing the wear induced nanocrystalline region above the UFG region is given in (A). A high magnification image from the nanocrystalline region is given in (B) with the accompanying SAED pattern from this location in (C). Next to the SAED pattern are half rings showing the measured d-spacing in nm, along with the closest corresponding orientation. The sliding direction is parallel to the top of each micrograph.

4. Discussion

4.1. Microstructural evolution and saturation in grain size and hardness at high equivalent strains

Many works have characterized the microstructural evolution after HPT processing to various amounts of equivalent strain [32]–[36]. Dislocations introduced by HPT processing accumulate into cells within grains that increase misorientation. When sufficient dislocations accumulate after a certain level of strain, misorientation becomes large enough that these formed cells become indistinguishable from grain boundaries. Then, after sufficient straining, a saturation microstructure develops due to a balance between further dislocation generation and recovery [48]. An early work on copper HPT noted that even at high strains, grain refinement ceased below an average of about 250 nm [49]. Various works have claimed that strains between 10 and 20 are sufficient for copper to reach an equilibrium grain size [34]–[36], [50]. From the SEM and TEM observations collected in the current work and shown in Figures 2.2 and 2.3, there are no indications that the present samples are significantly different compared to those from the literature.

While grain size may saturate after a certain amount of strain, the amount of high angle or twin boundaries may continue to evolve with further straining. Although grain size and hardness were seen to saturate at an equivalent strain of 15 in one work, it was noted that the fraction of high angle grain boundaries and average misorientation was still evolving [50]. In one EBSD investigation of pure copper HPT discs processed similarly to the current work, the mid radius of discs after 1 and 10 rotations both had similar average grain

sizes and high angle grain boundary fraction [33]. Conversely, the center of the 10 rotation disc was mostly the same, but the 1 rotation disc center had larger average grain size and lower high angle grain boundary fraction. Another work characterized twin boundary fraction, which was generally low (~5%) and homogeneous in 10 rotation discs whereas the 1 rotation discs had low twinning at the center and edge but upwards of 38% in the mid-radius [51].

In addition to grain size and misorientation, defect densities also change with the amount of strain. One work measured the distribution of vacancy clusters in HPT copper discs and found that higher rotations increased vacancy concentration with larger clusters found at the outer edge compared to the center [52]. The same work also measured dislocation density and saw only a minor increase with increasing rotations. Another work used finite element methods along with original and literature XRD and TEM measurements and saw evidence that dislocation densities saturate at equivalent strains less than 10 [53]. Some works have also documented the microstructural stability of HPT copper, which is important since the discs in the current work were characterized about two years after they were initially processed. After 4 weeks, discs processed to 10 rotations had a stable dislocation density of around 1.5×10^{-13} m^{-2}, while 1 rotation discs underwent recovery during that time and their dislocation density dropped by half from 6 $10^{-13}\times m^{-2}$ [54]. Thus, after 10 rotations saturation in grain size, grain boundary character, and defect density throughout the disc can be reasonably assumed, whereas a 1 rotation disc may have this saturation at the outer edge with large variation throughout.

The microhardness measurements in this study agree with several other works that have characterized copper processed by HPT and other SPD methods. Indeed, the hardening behavior of copper subjected to HPT follows from the same saturation in microstructure that was just described. HPT Cu hardness was seen to saturate around 130 HV after an equivalent strain of about 20 [55]. Copper processed by ECAE [56] and ARB [57] in the range of equivalent strains at which saturation occurs also reached around 130 HV. In the current work, the microhardness measured throughout the 10 rotation disc agrees with these values. The high microhardness in the low strain central region of the 1 rotation sample agrees with other studies that have investigated high purity copper samples aged at room temperature for times ranging from a few weeks to several years after HPT processing [51], [54], [58]. These works showed the occurrence of self-annealing at room temperature due to the relatively low melting temperature and stacking fault energy of high purity copper. This facilitated recrystallization in the outer edges of moderately strained discs due to higher stored energy there, while the low equivalent strain central portion remained unrecrystallized and with high hardness due to the compressive stress from the anvils. A decrease in dislocation density was seen around the mid-radius of discs processed to small ($\leq$1) rotations, corresponding to a sharp drop in hardness before steadily increasing again. For highly strained discs ($\geq$5 rotations), no drop in hardness was observed unless they had been aged for 7 years, after which a minor drop in the edges was found [58]. The discs in the current work were characterized two years after they were initially processed, so it is

reasonable that similar recrystallization is seen in our 1 rotation sample while no appreciable change is seen in our 10 rotation sample.

Thus, at the sufficiently high equivalent strain applied to the 10 rotation sample, the hardness, average grain size, ratio of high and low grain boundaries, and defect density is thought to saturate throughout the disc. As will be seen in the following sections, this property saturation for the 10 rotation disc is reflected by a saturation in wear properties at high strains. However some differences are also seen depending on wear path, an observation which requires further exploration and consideration.

4.2. Wear follows Archard scaling by decreasing with increasing equivalent strain and leveling off after saturation of microstructure and hardness, with a few notable exceptions

Figure 2.4 shows that normalized wear rate generally decreases with increasing equivalent strain up to around 15 at which prior works have seen a saturation in microstructure and hardness. The normalized wear rate levels off at around 0.25 after this strain, i.e. only about ¼ as much wear occurs after microstructural saturation as compared to the unprocessed condition. This trend follows the commonly-cited Archard relationship between hardness and wear resistance given by Equation 2, whereby copper that is work hardened through straining will have a reduced wear rate [37]. One work on copper processed by ECAE showed a consistent drop in normalized wear rate with successive passes [59]. Based on microstructural evolution in SPD materials, this result and those from the current work are unsurprising. Since increasing strain leads to grain refinement and Hall-Petch

strengthening, a sharp increase followed by a plateau in hardness should correspond with an inverse relationship for wear rate, as is illustrated in Figures 2.3 and 2.4.

However, a few works disagree with this trend between normalized wear rate and strain. Most glaring is the increased wear at high strains measured for 99.9% Cu processed by consolidating machined chips via HPT [21]. The original unprocessed coarse-grained copper conductivity in this work was only 71.7% IACS, suggesting that compositional differences were present even before any processing. It is possible that the machining and consolidation allowed further contamination from surface oxides to enter the microstructure. Embrittlement from oxides could have led to the higher wear rate measured. Another work by the same author on a Cu-0.35Cr-0.5Zr alloy also disagreed with the trends followed by the low strain works in Figure 2.4 [60]. In this work, increased wear and brittle fracture occurred at low strains since the elongated grains formed at this strain were easy to delaminate. Also, unlike the other alloy works in Figure 2.4, this composition has a supersaturation of Zr, so the zirconium left out of solution could have caused embrittlement. After 4 passes of ECAE, this zirconium may have been mechanically forced into solution giving rise to the “brittle to ductile” transition and increased wear resistance the authors observed at that processing condition. Such compositional issues encountered in these works are not well accounted for by normalizing the wear rate and make these works potentially unsuitable for comparison amongst the others.

The work on large strain extrusion machining (LSEM) in Figure 2.4 also shows wear behavior deviating from Archard scaling [61]. Machined chips were processed in this work at three increasing strains to create elongated nanograins, elongated/equiaxed nanograins, and equiaxed nanograins. Curiously, the greatest wear resistance was found for the lowest strain when the microstructure contained elongated nanograins. Wear rates were reported along three different sliding directions with differing results, although unfortunately these findings were not analyzed in terms of the microstructural response. In LSEM, strain is controlled by machining samples of different thicknesses, with thinner samples corresponding to higher processing strains. One possibility is that the higher wear rate seen for the high strain samples is an artifact caused by an interaction between the thinness of the sample and the experimental wear setup. It could also be possible that some aspect of the LSEM process introduced oxides or other contaminants into the microstructure. Although the authors stated that processing was slow enough to avoid heating, they do not state the speed used, and in their other works heating of 50-100°C even at low processing speeds was reported [62]. Either heating or oxidation could skew the results, or there could be more complex microstructural response as will be discussed further in the next section.

In Ni-W, another FCC system, wear has been shown to deviate from Archard scaling for grain sizes in the nanocrystalline regime [63]. Systematic investigation of pin on disc wear on nanocrystalline Ni-W showed that for the smallest grain sizes, less wear was seen than would be expected from Archard scaling. Wear rate consistently decreased with grain size, even at sizes below which the Hall-Petch relationship breaks down and hardness leveled

off. This was attributed to wear induced hardening from a combination of grain growth and grain boundary relaxation. Of the works in Figure 2.4, the electro-deposition work and the SMGT and SMAT works had grain sizes at or past the critical size for Hall-Petch breakdown in copper. Despite these small grains, the normalized wear rates for these works arrived at the same plateau as other high strain works with no indication of the Archard deviation seen for Ni-W. Thus, it is possible that wear induced hardening for extremely small grains does not occur for copper as it did for Ni-W. The difference could lie in the two-phase Ni-W having different wear modes compared to single phase high purity copper.

In sum, this work has provided a framework by which wear behavior can be assessed at a wide range of processing strains. By focusing on characterizing normalized wear rate as a function of equivalent strain, measurements from two HPT discs were collected that generally agreed with several other works spanning multiple processing conditions. This enabled observation of a saturation in wear rate, indicating that processing to strains higher than ~20 will not improve wear behavior. Similar testing can be conducted on other materials processed by HPT to improve knowledge of processing-structure-properties relationships with regards to wear. However, the simplicity of this approach comes with a few limitations. First, normalized wear rates only go so far in negating the influence of certain variables. Large differences in solute amounts, sliding speed, or normal force can significantly alter microstructural evolution and wear behavior. Second, equivalent strain calculation is often simplified and idealized and therefore has inherent limitations in describing the microstructures that are created by SPD. At the same equivalent strain, many

microstructural features like grain size, grain morphology, dislocation density, and twinning can differ for different processes, or as in the central region of HPT discs, there may be differences between the calculated and true equivalent strain experienced. Third, as with any comparative study, there are limitations based on what processing or characterization information is reported. Along with the myriad wear test parameters, a better accounting for wear track location in relation to processing textures and equivalent strains can greatly contribute to better understanding the origins of wear behavior in SPD materials.

4.3. Wear path influences wear rates after HPT or other directional deformation processes

The difference in wear rates between the radial and tangential tests in the current work indicates that track location and direction have a significant impact on the measured wear response for HPT discs. The higher normalized wear rates for the radial tests suggests that tracks covering a wider range of strains have a lower wear resistance. Such an observation might make sense for the inhomogeneous 1 rotation disc, but strangely it is also seen for the homogeneous 10 rotation disc. Since only one test was conducted for each location and no statistical analysis could be conducted, it is possible the difference in results between the radial and tangential tests are not truly significant. But, from other reports in the literature, there is enough indication that these results are significant enough to merit further exploration. In Figure 2.4, two works by Purcek et al. on Cu-0.7Cr-0.07Zr processed by HPT show a similar influence of wear path. These works used either continuous (ASTM G99) wear tests [20] at a radial distance of 5 mm or reciprocating

(ASTM G133) tests [29] centered at the same radial distance. The continuous test covered a smaller range of strains and had a comparatively lower wear rate, much like what was observed in the current work. The high strains used in their studies caused deformation induced solutionization, making it unlikely that the alloying additions are the main contributors toward the wear behavior they observed.

It is possible the discrepancy between these two works by Purcek et al. is due to a difference between continuous and bidirectional sliding. The LSEM work in Figure 2.4 also showed differences in wear rates between continuous and reciprocating tests, although without clear trends. Multiple prior works on coarse-grained aluminum, copper, and steel alloys have seen higher wear rates for unidirectional wear [64]–[66]. Some of these works attributed their results to the Bauschinger effect, by which a reversal in direction of an applied stress is accompanied by a decrease in yield strength. Strain hardening defects generated from stress in one direction may be annihilated upon the change in direction, resulting in softening. While these works did see a decrease in hardness after a few changes in direction in agreement with the Bauschinger effect, this softening did not manifest in an increase in wear rate as might be expected. The microstructures from HPT may have a complex interaction with the Bauschinger effect, thereby giving rise to the wear response seen in the current results and the two works by Purcek et al., but validating this would require further investigation. As a starting point, one computational study found the number of defects retained is higher in unidirectional sliding of single crystalline and nano-twinned microstructures, but not for nanograined copper [67]. Thus, it is possible that

changes in grain boundary character (i.e. twinning amount) for strained samples can be contributing to their wear response during continuous tests. This may also explain the unexpected trend between strain and wear rate for the LSEM work. Since the Bauschinger effect is essentially a microstructural response, it is vital to further discuss how wear behavior changes due to differences in microstructures encountered along wear tracks.

The influence of crystallographic orientation on wear response can be inferred from some of the data in Figure 2.4, and it has also been described in works on other materials over the years. In the current work, due to the shear texture that forms in HPT discs, the tangential tests with lower wear rate are more parallel to the shearing direction, whereas the radial tests with higher wear rate are entirely perpendicular to the torsional shearing. One work from NASA in 1969 reported that 50% rolled aluminum displayed lower wear when slow, mild sliding was normal to the rolling direction compared to parallel [68]. The work on extruded copper included in Figure 2.4 also showed decreased wear rate when disc on shoe sliding was parallel to the extrusion direction with an increase in wear rate for perpendicular sliding [69]. A work on an aluminum alloy processed by ECAP also had different wear rates when parallel or normal to the deformation axis [70]. In a work with polycrystalline cold rolled/drawn steel pins worn on steel discs, changes in wear properties were observed depending on the orientation with which the pin was cut, and a higher wear rate was seen when sliding was parallel to the rolling or drawing direction [71]. Another work on single crystals of copper noted differences in wear particle formation depending on the orientation of the shear plane in relation to the sliding [72]. The influence of texture

on wear and vice versa has been studied in a series of works using bronze alloy pins in continuous pin on disc wear tests by Cai et al. Recently they quantitatively described strain accumulation and grain rotation for single crystal and coarse grained polycrystalline pins [73]. All of these results point toward the existence of a unified explanation for the crystallographic influence on wear properties, one area that tribologists in the SPD community are uniquely equipped to investigate.

While the current work has focused on post mortem determination of wear rates after dry sliding wear, another related work monitored changes in deformation behavior due to lubricated sliding on metals processed at different initial strains [74]. This study used *in-situ* video of a lubricated wedge sliding across aluminum samples at initial strains from 0 to 2 to determine the mesoscale strain accumulation after a single pass. The authors characterized the microstructural response in the wake of this sliding as "laminar" for these low strains, and higher initial strains incurred a breakdown in this smooth response, with folds or localized shear bands created instead. Formation of such inhomogeneities leads to material removal and increases wear rate. Another computational work eschewed the flow-like treatment of fold formation, and instead presented evidence that bulging is a crystallographic response by grains of ideal orientations with respect to the sliding force field [75]. It is possible that the shear textures imposed by HPT processing may be better oriented for bulge formation when sliding in certain directions, but more work needs to be done to verify this.

Outside of the SPD community, the work done by Greiner et al. has illuminated the microstructural response during early stages of dry sliding for coarse grained copper [45]. The coefficients of friction in that work are in the same range as those in the current work, further validating that mild sliding was achieved despite different test parameters. One important feature of this work is that it has shown that dislocations injected from the wear surface accumulate in the microstructure due to sliding, forming a "dislocation trace line" a certain depth below the surface. A better understanding of this dislocation trace line formation in relation to any potential Bauschinger effects is needed. The formation of amorphous oxygenated clusters at the wear surface in early sliding was also reported in this work, observing a pathway by which oxygen enters the nanocrystalline layer, as was observed from the SAED in the current work. Recently, the same research group has reported another dry sliding study using coarse grained copper membranes with different aspect ratios to investigate differences in tribology with strain [76]. This membrane work analyzed strain during sliding as opposed to the current work which analyzed initial processing strain. They found that membranes with higher aspect ratios experienced more strain during sliding and exhibited lower COF and less geometrically necessary dislocations in the subsurface microstructure. Insight gained on the fundamental processes in wear of coarse-grained materials can be applied toward understanding wear of fine-grained materials and vice versa to improve basic understanding of wear mechanisms across all grain sizes.

To summarize, researchers should be aware that different test locations can give different measurements of wear response in HPT discs. This should be kept in mind when designing wear studies, reporting results, and comparing the results of others. Prior works on SMAT and other surface deformation techniques have probed the wear response of materials with large gradients in equivalent strain and grain size below the tracks. This work is unique in analyzing the wear response of samples with a variety of such gradients along the length of the track. Since HPT produces materials with substantial radial inhomogeneity, they are prime candidates for exploring tribological response across nonuniform microstructural regimes. Further research can more comprehensively probe the microstructural response when sliding wear traverses a wide range of grain sizes.

5. Conclusion

This work has examined variations in wear rate with respect to equivalent strain in HPT processed copper discs. Microstructural saturation after processing past an equivalent strain of about 15 reduced wear rate by about 75% compared to unprocessed copper. Additionally, discrepancies between linear reciprocating wear tests conducted at different regions of the same disc has indicated that wear resistance is dependent on a relationship between strain path and wear path. Wear measurements gathered only from 1 and 10 rotation HPT discs agreed with values from the literature for various SPD conditions. The incremental microstructural and wear evolution shown for high equivalent strains indicate that materials receive no tribological benefits from higher SPD strains.

Acknowledgements

HPT was carried out in the International Research Center on Giant Straining for Advanced Materials (IRC-GSAM) at Kyushu University, Japan. Scanning electron microscopy was performed on a FEI Nova NanoSEM 450 in the Central Facility for Advanced Microscopy and Microanalysis (CFAMM) at UC Riverside. Focused ion beam was performed on a ThermoFisher Scientific (formerly FEI/Philips) Quanta™ 3D 200i in the CFAMM at UC Riverside. Transmission electron microscopy was performed on a ThermoFisher Scientific (formely FEI/Philips) Titan Themis 300 and an FEI Tecnai T12 in the CFAMM at UC Riverside. EHR was supported by the GAANN Fellowship from the Department of Education through the Mechanical Engineering department at the University of California, Riverside. SNM was supported via NSF CMMI Grant # 1663522.

Chapter 2

Electrical conductivity characterized at varying strains in spiral cut high-pressure torsion discs

Evander Ramos[a], Takahiro Masuda[b], Zenji Horita[b], Suveen Mathaudhu[a,c]*

[a]University of California, Riverside, USA

[b]Kyushu University, Fukuoka, Japan

[c]Colorado School of Mines, USA

* Corresponding author: smathaudhu@mines.edu, 1500 Illinois St., Golden, CO 80401, USA

Abstract

High-pressure torsion (HPT) imparts inhomogeneous strain to process discs with low strain in the center and higher strain at the outer edge. Microscopy and microhardness indentation have been used to characterize and correlate this inhomogeneity with strain, but similar exploration with other properties has been uncommon. In this work, the electrical conductivity of pure copper discs processed by HPT was characterized with respect to equivalent strain by cutting them into spirals with an incremental, monotonic increase in strain. Electrical conductivity varied with straining in agreement with the literature and

expectations based on grain boundary evolution. The spiral conductivity testing method outlined in this work can improve characterization of HPT materials in future studies.

Keywords: Ultrafine-grained, copper, high-pressure torsion, severe plastic deformation, equivalent strain, electrical conductivity.

1. Introduction

High-pressure torsion (HPT) is a well-documented severe plastic deformation (SPD) technique with the potential to impart large strains, albeit inhomogeneously. This inhomogeneity arises from the torsional straining, which can be described by the equation $\varepsilon = \frac{2\pi rN}{\sqrt{3}\,t}$, where ε=equivalent strain, r=radial distance, N=number of rotations, and t=thickness [55]. Microscopy and microhardness indentation at discrete locations throughout samples have been used to characterize inhomogeneity with processing strain. However, some properties are characterized via tests across large volumes encompassing wide ranges of strains, thereby obfuscating their evolution with processing.

Electrical conductivity in HPT discs has been characterized via four-point probe in tests across cut strips [55], [77]–[79] or co-linear surface tests [80], [81], eddy current techniques [82], and across entire samples [21], [83]. Most works report single values for the conductivity of discs, disregarding inhomogeneity across the specific tested regions. Only a few works have explicitly incorporated inhomogeneity in characterizing conductivity across discs [77]–[80]. However, these tests suffer from inflexibility in probing different strain levels and measurement errors due to small sample sizes. Thus,

improved testing methods are necessary for more versatile and accurate strain-based conductivity characterization of HPT samples.

In this work, HPT processed pure copper discs were cut into uniform spiral wires with monotonically increasing equivalent strain to probe conductivity. Measurements between specific strain ranges enabled accurate conductivity characterization across discs. Pure copper was used for its relevance in electrical applications, along with the wealth of SPD literature available for comparison. The results gathered agreed with SPD literature, demonstrating the improved efficiency and precision of this spiral conductivity testing method for characterizing variations with strain in HPT discs.

2. Materials and Methods

Discs of high purity copper were processed in a prior report, where microhardness and microstructures at varying strains were also characterized [84]. In this work, an electrical discharge machine was used to cut these discs into an Archimedean spiral shape with a uniform 0.6 mm square cross section. This shape facilitated electrical conductivity characterization using a four-point probe technique with a Keithley 2636B SourceMeter. As illustrated in Figure 3.1a, two DC source leads were placed at the center and outer section of the spiral and two voltage sensing leads were placed at varying points along the spiral to measure the response at different sections (colored red, blue, and green) as well as for the entire length. Tests used a current of 1 Amp at room temperature. The current density applied during these tests was four orders of magnitude below the threshold for electromigration, so microstructural changes during testing was negligible [85]. Current

reversal and line cycle integration were used to cancel out thermoelectric electromotive force and power-line noise, respectively, as recommended for low-voltage measurements [86]. Resistivity was determined from the uniform cross-sectional area and the length between probes. Error propagation was calculated as the root sum squared combination of the measurement uncertainty of the wire thickness, width, and length, as well as the uncertainty between five measurements for each section. Due to physical constraints necessary to cut the spirals, the centermost and outermost regions of the discs were excluded from characterization.

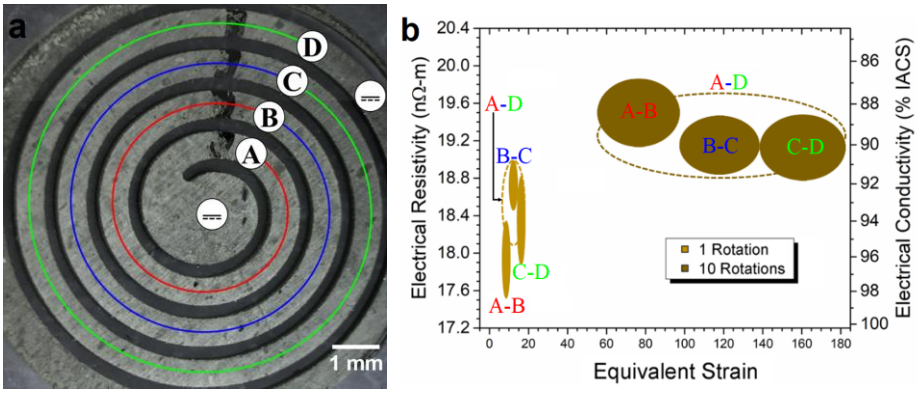

Figure 8: (a) Spiral cut HPT disc overlaid with the locations of the current source probes (⎓) and voltage sense leads (A-D). (b) Electrical resistivity and conductivity variation with equivalent strain for the three spiral sections (solid filled) and the entire spiral (dashed) for 1 and 10-rotation discs. The y-spread is the standard error of the measurements, while the x-spread is the range of equivalent strains covered by the tested section.

3. Results and discussion

3.1. Spiral conductivity testing method results

The results of the conductivity tests are shown in Figure 3.1b, with the conductivity of pure copper, nominally 100% IACS (International Annealed Copper Standard), near the x-axis.

The conductivities for the entire spirals (A-D) of the 1 and 10-rotation discs were 93.2±2.1% and 89.5±2.1% IACS, respectively. Combining the individual measurements from the three spiral sections gave 93.8% and 89.7% IACS for the 1 and 10-rotation discs, respectively, corresponding well with the entire spirals. Generally, the entire spiral covers a wide range of equivalent strains, much like in prior reports testing conductivity across cut HPT strips or entire discs. The high conductivity measured for the innermost tested 1-rotation region (A-B) lies outside the error bars for the entire spiral, so essentially, had traditional conductivity testing been used, this behavior would not have been observed. The 1-rotation sample had an average grain size of 700±200 nm, while the 10-rotation sample had an average of 290±150 nm, as shown previously [84] and in agreement with published literature [55]. Using an approximation of grain boundary contribution to electrical resistance in copper at room temperature [87], resistance should increase by about 1.0 nΩ-m and 2.5 nΩ-m for the 1 and 10-rotation discs, respectively, in line with the values presented in Figure 3.1b.

3.2. Comparison to SPD literature

The present results were compared across the SPD copper literature in Figure 3.2. Prior works measuring conductivity after cycles of accumulative roll bonding [88] and equal channel angular extrusion [56] agreed with the measurements from the 1-rotation disc. Another HPT work conducted four-point probe testing on strips cut from many discs, which agreed with the values measured presently from just two discs. Linear extrapolation of the results from these two discs gave an inflection point for conductivity at an equivalent

strain around 25, with a minimum value of 87.5% IACS. This agrees with the literature, where a strain of around 20 has been cited as the onset of saturation in hardness and microstructural evolution in copper [55], [84]. Although the 10-rotation disc error bars overlap, they show a slight increase in conductivity with equivalent strain, which was also indicated in the prior work [55]. The hardness saturation noted from the literature past a certain strain reflects a saturation in dislocation density, but rearrangements of the dislocation structures may still occur [2]. Consolidation of dislocation tangles toward more defined grain boundaries can result in an overall increase in conductive pathways and explain this slight increase in conductivity. More exploration is required in the future to determine the limits of this conductivity evolution at high strains.

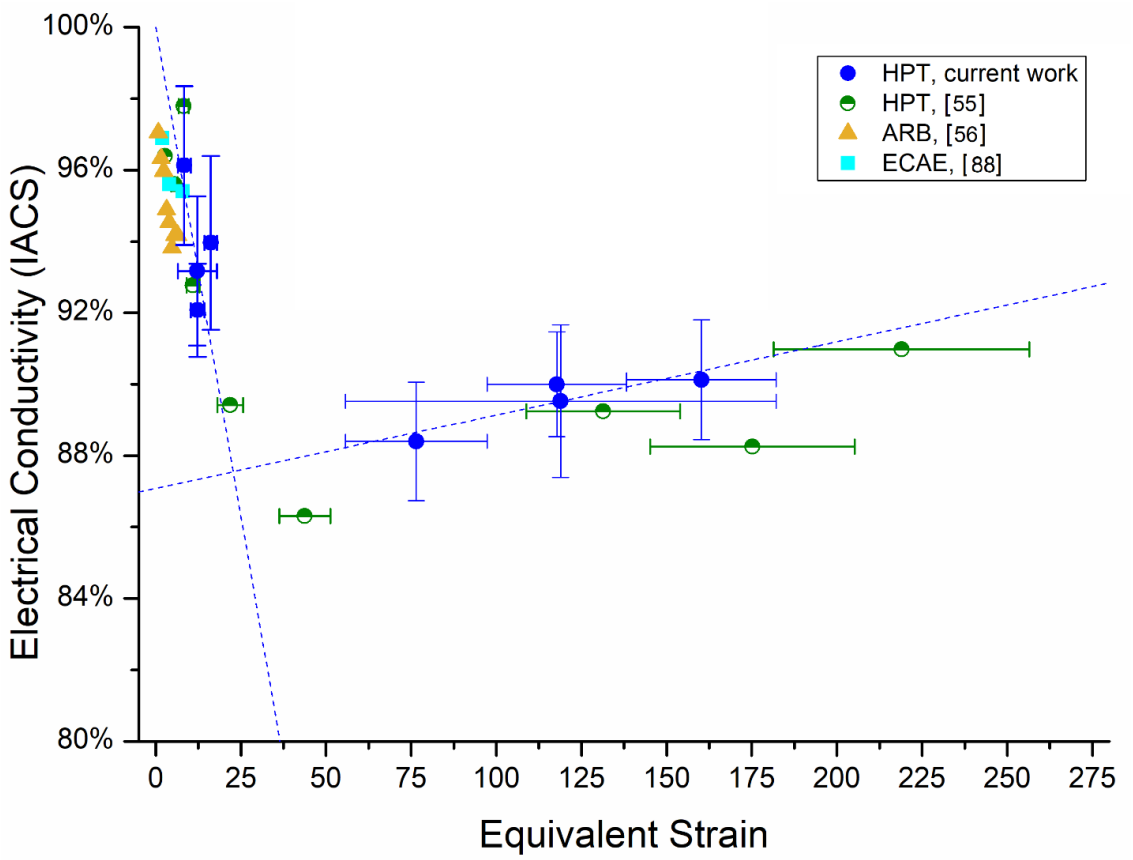

Figure 9: Electrical conductivity variation with equivalent strain in the present work and other SPD studies. All works *[55], [56], [88]* used 99.99% Cu. Trendlines for the two discs in the current work are also included.

3.3. Comparison to other strain-based testing methods

Only a few works have characterized conductivity with strain throughout individual HPT samples. Another Cu work [78] used a four-point probe method on small sections cut from disc diameters, but they also measured grain boundary length at varying strains and saw no correlation with conductivity. One explanation for this could be the measurement procedure itself. With characterization conducted on 1 mm strips, inaccuracy in measuring such a short length would potentially contribute a large percentage of error for resistivity

calculations. In the present work, the shortest spiral section was much longer, and exhaustive efforts were implemented to mitigate and calculate the propagation of error. Another prior work used colinear four-point probe testing to map conductivity throughout titanium and zirconium discs [80]. Unfortunately, variation in geometric correction factors with probe placement adds variability to such mapping, especially near the sample edge. In another work, ring samples processed by HPT were cut concentrically like a bullseye to characterize conductivity at three short ranges of equivalent strain [79]. Another recent work explored thermoelectric properties throughout large HPT samples using a few small cut strips [77]. The testing methods used in the present work allow for greater flexibility to probe across broader strain ranges than in these two works. Thus, compared to prior literature characterizing conductivity in different regions of HPT samples, the spiral conductivity testing method used in the present work provides an accurate and efficient framework for exploring electrical behavior with strain.

4. Conclusion

Electrical conductivity in copper discs processed by HPT was probed with respect to equivalent strain through spiral cutting and four-point probe testing. Measurements gathered from 1 and 10-rotation discs agree with values from the literature for copper after various SPD processes and conditions. The spiral conductivity testing method showcased in this work can improve assessment of processing-structure-property relationships in other materials, such as alloys, nanocomposites, and thermoelectrics.

Acknowledgements

HPT was carried out in the International Research Center on Giant Straining for Advanced Materials (IRC-GSAM) at Kyushu University, Japan. EHR was supported by the GAANN Fellowship from the Department of Education through the Mechanical Engineering department at the University of California, Riverside. SNM was supported via NSF CMMI Grant #1663522.

Chapter 3

Microstructural origins of the anisotropic wear response of copper processed by high-pressure sliding

Evander Ramos[a], Takahiro Masuda[b], Yoichi Takizawa[c], Zenji Horita[b], Suveen Mathaudhu*[ade]

[a] Department of Mechanical Engineering, University of California, Riverside, United States
[b] Department of Materials Science and Engineering, Kyushu University, Fukuoka 819-0395, Japan
[c] Technology Department, Nagano Forging Co., Ltd, Nagano, Japan
[d] Department of Materials Science and Engineering, University of California, Riverside, United States
[e] Department of Metallurgical and Materials Engineering, Colorado School of Mines, United States

* Corresponding author: smathaudhu@mines.edu, 1500 Illinois St., Golden, CO 80401, USA

Abstract

A better mechanistic understanding of how microstructural features such as grain size and morphology affect wear can inform ways to address important tribological problems. Reports on wear test results on a number of materials processed via directional straining indicate that a relationship exists between wear path and strain path. Severe plastic deformation techniques are potentially useful for exploring and validating such strain-based observations of material behavior. In this study the directional dependence between wear and strain is explored in copper processed by high-pressure sliding, a severe plastic deformation technique that imparts unidirectional shear. Differences between wear rates

for dry sliding conducted parallel and perpendicular to the processing strain are noted. Microstructural mechanisms underpinning these differences in wear are advanced based on review of the severe plastic deformation literature.

Introduction

Despite its relevance to many technologies such as energy, transportation, and public health, a complete understanding of the microstructural basis for wear is currently lacking. Recent exploration of dry sliding wear on coarse grained copper has led to some advances in understanding mechanisms in the early stages of wear [45], however in the later stages, surface sliding imparts significant microstructural refinement throughout the wear-affected region, creating a nanocrystalline near-surface layer, below which are ultrafine grains (UFG) (100 nm – 1000 nm average grain size) [89]. Since wear is essentially a large-strain deformation process [90], tribological studies on materials processed by severe plastic deformation (SPD) techniques, such as high-pressure torsion (HPT) and equal channel angular extrusion (ECAE), may inform and represent microstructural evolution in the later stages of sliding wear.

Prior studies of wear in SPD materials has yielded conflicting reports at times, so further research is necessary to illuminate the microstructural basis for these discrepancies [12]. For example, wear studies of commercial purity titanium have variously indicated that wear rates either decrease after ECAE [91] or HPT [27], increase after hydrostatic extrusion [92], or even that there is no significant effect from ECAE [93]. A prior work by the authors

explored some of these inconsistencies in the literature and found evidence that wear resistance in copper generally increases with processing strain and saturates after an equivalent strain of about 15 [84]. Moreover, the authors also found evidence that wear rates differed when the sliding tests traversed along different orientations with respect to the initial shear processing direction. Linear reciprocating tests from the center to the edge of HPT discs (perpendicular to the circumferential shear processing direction) showed higher wear rates than identical tests centered about different radial distances (more parallel to the circumferential shear processing direction). This was indicated from only a single test at each condition due to the limited space available for testing on HPT discs, making interpretations of the significance of the results challenging, if not impossible. Further testing is warranted to investigate the hypothesis that wear rates increase when measured perpendicular to the shearing direction during SPD.

A newer SPD method that has been developed is high-pressure sliding (HPS), which is a linear analogue to HPT [94]. Similar to ECAE route A where there is no billet rotation in between extrusion passes [95], shear stress is applied uniformly throughout the processing, although HPS instead accumulates strain faster and without the need for multiple passes. For example, while ECAE can impart an equivalent strain of ε=1.15 per pass [95], the HPS process can impart ε=4.1 in a 0.8 mm thick sample after a plunger displacement of 5 mm [94]. Further, the large volumes of material that can be processed by HPS as compared to HPT enable more representative wear testing to be conducted for statistical validation of trends. Additionally, the linear shear path enables more idealized wear path testing that is

either parallel or perpendicular to the applied shear, as compared to the complex, not entirely parallel wear path for the prior circumferential shear imparted by HPT.

In the present work, characterization of pure copper processed by HPS has been conducted for comparison with findings from the extant SPD literature. Microstructural characterization has been conducted on copper processed by HPS to assess similarities and differences. Wear testing was then conducted parallel and perpendicular to the processing (sliding) direction. Multiple wear tests were conducted to lend significance toward testing the hypothesis that wear rates increase when measured perpendicular to the shearing direction. The findings of this study do indeed validate this hypothesis, and are presented alongside discussion of a number of relevant prior reports that further reinforce this relationship between wear path and shear path.

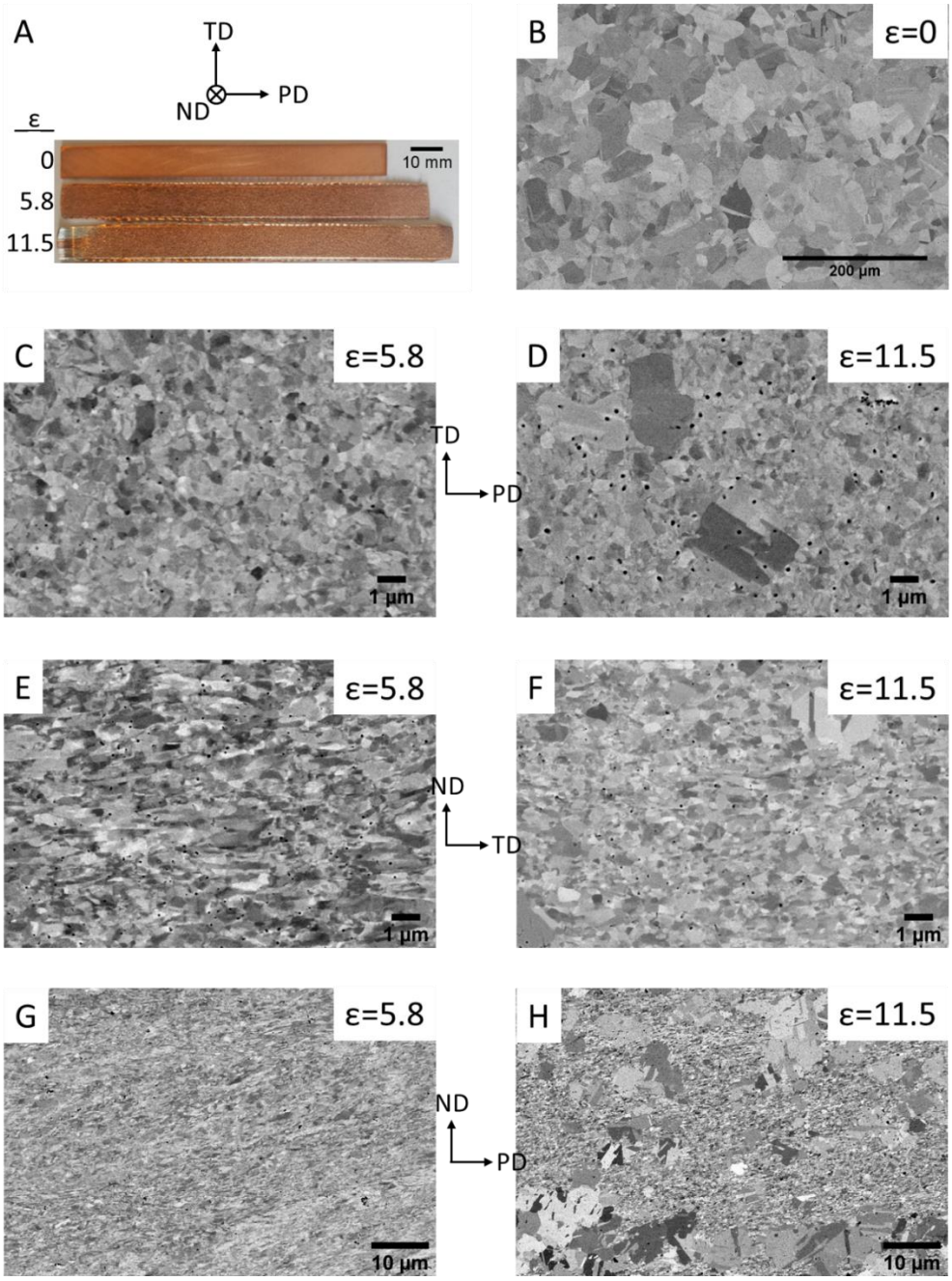

Figure 10: (A): Image of as unprocessed and processed samples from both strained conditions along with the total equivalent processing strain for each condition; (B): Unprocessed copper microstructure showing large initial average grain size (>20 μm); (C), (E), and (G): Microstructures of the ε=5.8 sample; (D), (F), and (H): Microstructures of the ε=11.5 sample. Images (C) and (D) are in the plane of the samples (plane perpendicular to ND), while (E) and (F) show a cross section (plane perpendicular to PD), and (G) and (H) show the other cross section (plane perpendicular to TD).

Materials and Methods

High purity copper (99.99%) was processed by high pressure sliding in accordance with methods reported previously [94]. Two copper strips with initial nominal dimensions of 100 x 10 x 1 mm^3 were compressed to 2 GPa on either side of a grooved plunger, as can be seen in Figure 4.1 of [94]. Sliding was conducted at room temperature by pushing the plunger at a constant speed of 1 mm/min for two sets of sliding distances, 10 and 20 mm. These processing conditions correspond to equivalent strains of 5.8 and 11.5 according to the equation $\varepsilon = \frac{x}{t\sqrt{3}}$, where x=sliding distance and t=initial thickness [94]. An unprocessed control sample was also used for comparison, and the three samples are shown in Figure 4.1a. Also indicated in the figure are the directions that will be referred to throughout this paper, namely the processing direction (PD), transverse direction (TD), and normal direction (ND).

Metallographic sample preparation, microscopy, Vickers microhardness indentation, and linear reciprocating wear testing were conducted identically to a prior work by the authors on HPT Cu, except as indicated in this paragraph [84]. Electropolishing reduced the surface roughness (R_a<100 nm) for improved microscopy and wear testing. Images for grain size determination were collected using scanning electron microscopy conducted perpendicular to the normal direction at 20 mm intervals along the processing direction. Vickers microhardness was also conducted to gauge homogeneity by making five indentations across the transverse direction every 10 mm along the processing direction. Electrical conductivity testing was conducted using a four-point probe technique with a Keithley

2636B SourceMeter. Five measurements were taken at room temperature with a current of 1 A on a 50 mm section in the middle of each strip.

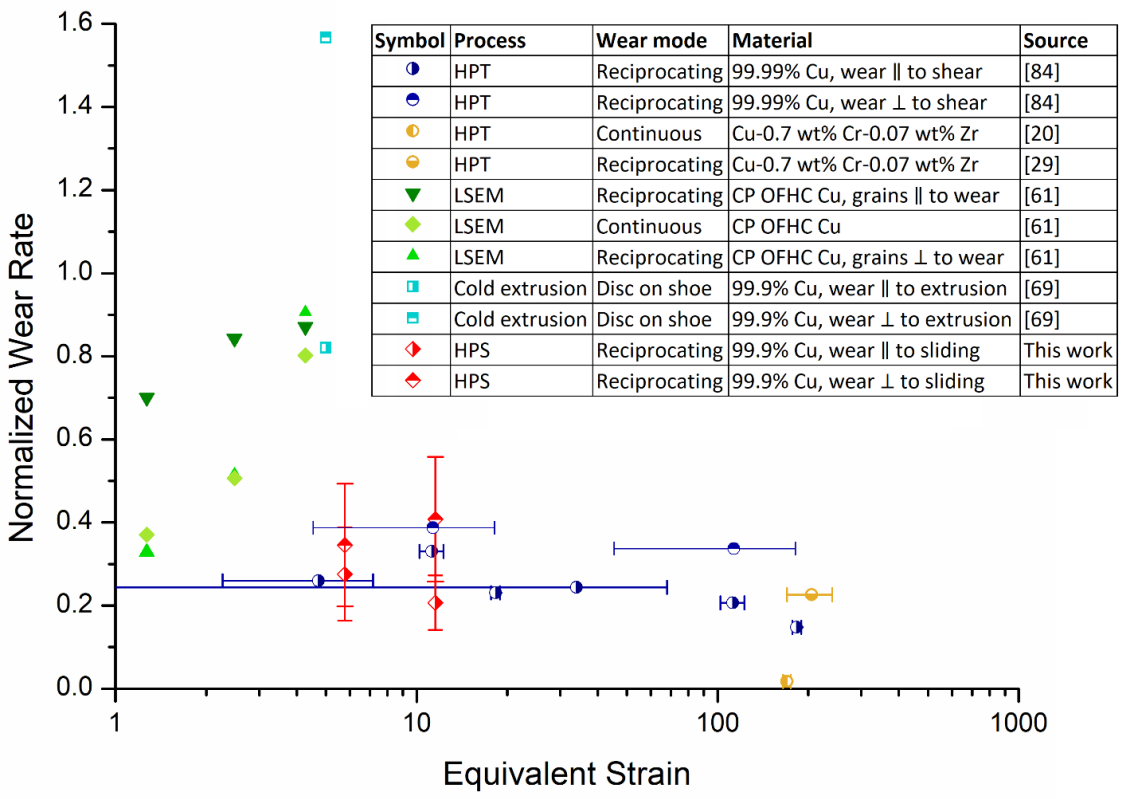

Symbol	Process	Wear mode	Material	Source
	HPT	Reciprocating	99.99% Cu, wear ∥ to shear	[84]
	HPT	Reciprocating	99.99% Cu, wear ⊥ to shear	[84]
	HPT	Continuous	Cu-0.7 wt% Cr-0.07 wt% Zr	[20]
	HPT	Reciprocating	Cu-0.7 wt% Cr-0.07 wt% Zr	[29]
	LSEM	Reciprocating	CP OFHC Cu, grains ∥ to wear	[61]
	LSEM	Continuous	CP OFHC Cu	[61]
	LSEM	Reciprocating	CP OFHC Cu, grains ⊥ to wear	[61]
	Cold extrusion	Disc on shoe	99.9% Cu, wear ∥ to extrusion	[69]
	Cold extrusion	Disc on shoe	99.9% Cu, wear ⊥ to extrusion	[69]
	HPS	Reciprocating	99.9% Cu, wear ∥ to sliding	This work
	HPS	Reciprocating	99.9% Cu, wear ⊥ to sliding	This work

Figure 11: Plot of normalized wear rate vs. equivalent strain from the current work and for a number of other studies on different SPD processes. All results show differences in wear behavior based on sliding direction in relation to processing direction. *[20], [29], [61], [69], [84]*

Three wear tests were conducted for each of two orientations, parallel and perpendicular to the direction of the processing sliding (i.e. processing direction and transverse direction, respectively). All wear tests were conducted in air at a relative humidity of 37±7% and at room temperature (22.9±1.3°C) within a small 8 mm section in the middle of each strip.

The resulting wear tracks were cleaned with compressed air and evaluated using a Nanovea profilometer with analysis software to determine the profile of the scar with ≤25 μm resolution parallel to the track and 1 μm resolution perpendicular to the track. Specific wear rate was calculated by dividing the measured wear volume at the conclusion of the test by the total sliding distance and load. Furthermore, normalized wear rate was calculated by dividing the wear rate of the processed tests by that of the unprocessed control, in order to determine the relative influence of the processing method on wear behavior. To assess microstructural evolution due to wear, two foils were extracted from the 11.5 equivalent strain strip using the FIB lift-out technique: one from the center of a perpendicular wear track and one from the center of a parallel wear track. These foils were extracted about 8 months after the wear test was conducted. Another two foils were extracted parallel to these but far away from the wear tracks to characterize the bulk microstructures for comparison. These foils were imaged using a Talos L120C TEM at 120kV.

Results

Microstructure, microhardness, and electrical conductivity typical of SPD copper

Figure 4.1a shows the three samples examined in this study: unprocessed (0 strain) and processed to 10 and 20 mm (equivalent strain of 5.8 and 11.5, respectively). The corresponding representative microstructures for these samples are shown from images taken perpendicular to the normal direction in Figures 4.1b-d, perpendicular to the processing direction in 1e-f, and perpendicular to the transverse direction in 1g-h. For

brevity, only one representative image was included in Figure 4.1 for each sample and orientation. While grains appeared mostly equiaxed in the plane perpendicular to the normal direction, in the other imaged planes they appeared elongated. The average grain size perpendicular to the normal direction was relatively static across the imaged sections of the strips, which also corresponded to uniform microhardness measurements throughout, as shown in Table 1. However, due to the aforementioned elongation, the actual grain size is larger. The higher strain condition ($\varepsilon = 11.5$) shows less elongation, but also some larger grains scattered throughout and seen in all planes of viewing. This is also reflected in the microhardness, as the scattered larger grains caused a higher deviation in the values for the higher strain strip as well as a slightly lower average, whereas the lower strain ($\varepsilon = 5.8$) strip had a smaller deviation. The electrical conductivity measured for each sample is also included in Table 1. The values of 94.5±2.6 and 88.2±1.4 %IACS for the processed conditions generally scales with the amount of strain applied.

Wear rate shows dependence on sliding direction in relation to processing direction

Wear behavior for all samples and directions is included in Table 1. For all samples, differences are observed when sliding is parallel or perpendicular to the processing direction. Figure 4.2 shows this dependence in comparison to other works that have displayed similar dependence on wear direction. Altogether, it appears there is mounting evidence that wear will decrease when measured perpendicular to highly strained materials.

Table 1: Grain size, microhardness, electrical resistivity, and wear properties for the three strips.

Equivalent Strain	Average Grain Size (μm)	Vickers Microhardness (HV (kgf/mm^2)	Electrical Resistivity (nΩm)	Specific Wear Rate (mm^3/Nm)	Steady State COF
0	20	47.7 ± 4.1	17.3 ± 0.18	PD: 8.2E-05 ± 2.2E-05	PD: 0.55
				TD: 5.9E-05 ± 2.1E-05	TD: 0.58
5.8	0.313 ± 0.030	136.5 ± 0.7	18.2 ± 0.65	PD: 2.3E-05 ± 6.9E-06	PD: 0.52
				TD: 2.1E-05 ± 4.9E-06	TD: 0.54
11.5	0.378 ± 0.053	132.4 ± 2.5	19.5 ± 0.43	PD: 1.7E-05 ± 2.8E-06	PD: 0.55
				TD: 2.4E-05 ± 2.5E-06	TD: N/A

The wear tests perpendicular to the processing direction (in the transverse direction) have higher normalized wear rates, indicating a lower wear resistance in this direction. This difference is more significant in the higher strain condition. The microstructures that developed below the wear tracks of the higher strained strip are shown in the foils in Figure 4.3. From grain size analysis of the grains near the bottom of these foils, it is apparent that some coarsening occurred from the original grain sizes shown in Figure 4.1 after wear testing. Direct comparison of the apparent coarsening of the microstructures extracted from elsewhere on the strips and from the center of the wear tracks for each orientation gave a change from 0.32±0.12 μm to 0.53±0.18 μm for the perpendicular foils and from 0.32±0.10 μm to 0.74±0.31 μm for the parallel foils. Essentially, from measuring elongated grains of similar sizes, it can be interpreted that wear testing drove the grains to coarsen at different magnitudes based on a difference in sliding direction. However, it should be noted that the

overlap between the error bars for the two grain coarsening measurements is significant, and these measurements were taken from only two extracted foils, therefore no definative statements can be made on the grain coarsening behavior below wear tracks at different orientations, but these results expose a potential relationship that future works can explore more thoroughly.

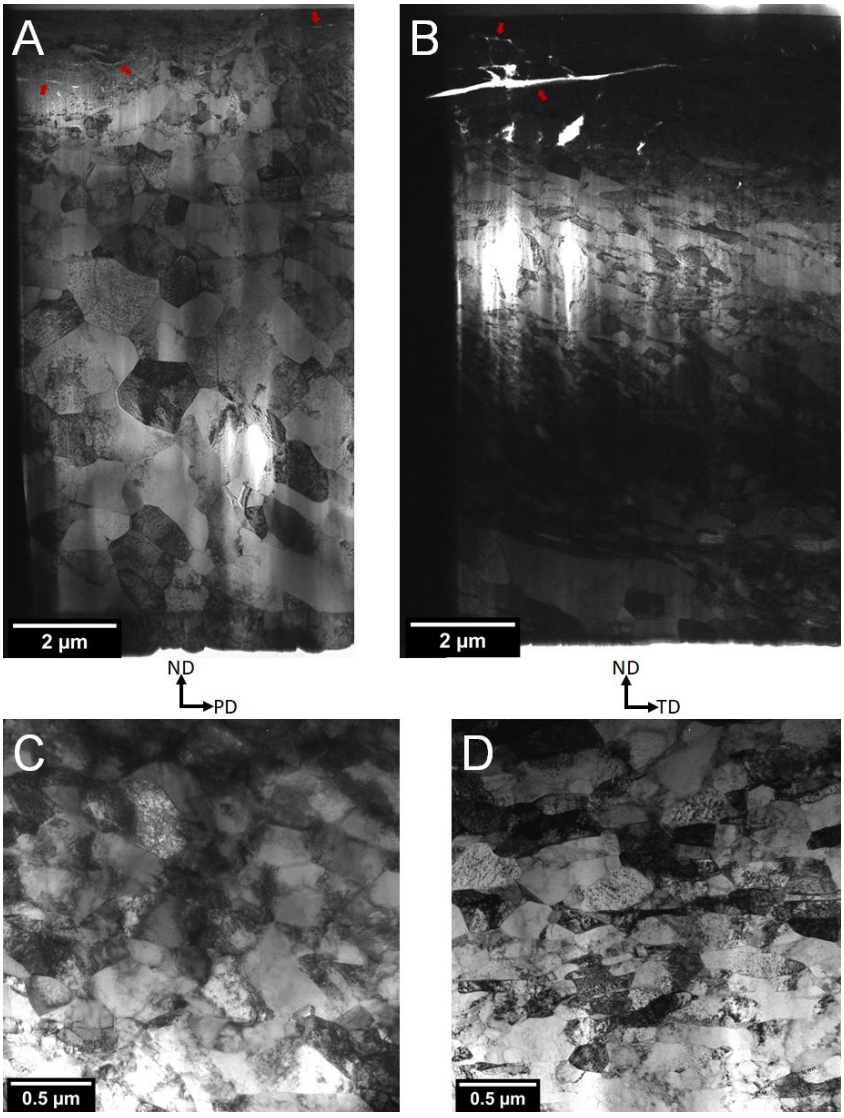

Figure 12: Foils extracted from the center of the “parallel” wear track conducted along the processing direction (A) and for the “perpendicular” wear track conducted along the transverse direction (B). These foils were extracted from the plane perpendicular to the

transverse direction (A) and from the plane perpendicular to the processing direction (B). Each foil is oriented with the wear surface at the top (with the protective carbon layer visible just above) and with the side attached to the TEM grid on the left. Small arrows point out what may be wear induced cracks just below the wear surface. For comparison, representative bulk microstructures from foils extracted in the same orientations but far away from the wear tracks are shown for the plane perpendicular to the transverse direction (C) and perpendicular to the processing direction (D). The structure in (C) corresponds with that of figure 4.1H, while the structure in (D) corresponds to 1F.

A few other observations can be made from the microstructures shown in Figure 4.3. The depth of the nanocrystalline near surface region is variable for the wear track parallel to the processing direction, having a "wavy" profile with an average depth of ~1.3 μm. Immediately below the surface after wear testing, the grains have an average size of 10±5 nm, in line with prior observations of the extreme grain refinement possible in worn surfaces [46]. The nanocrystalline layer in the foil for the wear track perpendicular to the processing direction (Fig. 3b) is unfortunately too thick in the near surface region to allow the necessary electron transparency in the TEM. This foil was left thick at the wear surface because a hole was seen to form in this region during thinning with the FIB, so it was not subsequently milled to avoid further damage. Upon viewing in the TEM, this hole was revealed to be a nominally 5 μm long crack running at an angle of between 4 and 8° from the wear surface (indicated with an arrow on Fig. 3b). In the other subsurface wear foil, some cracking is also be seen, but to a much lesser extent. The significance of these observed cracks is difficult to interpret, as it is possible they are simply the result of damage during the FIB process. Cracking in both foils occurred near where the foils were attached to a TEM grid, so it is also possible that the cracks are a result of residual stresses from the foil mounting. Any residual stresses could either have created cracks or exacerbated existing ones. Beam damage from the Ga ion gun is also a possibility, although this too

could either have created or exacerbated existing cracks. No such surface cracks were visible in the foils extracted from outside of the wear tracks (Figs. 3c and 3d). These cracks remain inconclusive and in need of further study to better understand the root cause of their formation, and more so if these can be attributed to the microstructural anisotropy that informs wear behavior.

Discussion

Microstructures, microhardness, and electrical conductivity agree with prior SPD Cu literature

No obvious disagreements are found when comparing copper processed by more established SPD processes with the current characterization of HPS processed copper. From the representative images in Figure 4.1, it is clear the grains are not equiaxed, but rather elongated in the sliding direction, in line with prior observations of low strain SPD processed copper [2], [34]. Additionally, since our work is not on ultra-high purity copper, the relative stability of the ~300 nm grains may be assumed to be due in part to any impurities or oxygen pinning grain boundaries [96]. Such grain boundary doping (possibly due to impurities from the WC-Co wear test ball) is certainly more prevalent in the nanocrystalline layer just below the wear surface, which has maintained a ~10 nm average grain size even 8 months after wear testing. Prior reports on HPS have consisted of a number of different aluminum alloys [94], [97], and it is possible the difference in stacking fault energy for these aluminum-based samples (γ_{SFE} = 166 mJ/m^2) and Cu (γ_{SFE} = 78

mJ/m^2) give rise to different microstructural evolution and the elongation observed here [98].

Another interesting feature of the micrographs is the grain growth displayed in the higher strained ($\varepsilon = 11.8$) sample. For SPD processing, input strain may reach a point where it contributes toward dynamic recrystallization instead of grain refinement. With further straining, an equilibrium can be reached between the rate of dynamic recrystallization and refinement of recrystallized grains, leading to an onset in saturation of microstructural evolution. For copper, this has been measured to be around an equivalent strain of $\varepsilon = 20$ [55]. Since the higher strained HPS strip is not yet at this strain, it is plausible that the large recrystallized grains are nucleating without being significantly refined further.

The hardness and average grain size shown in Table 1 matches well with prior literature from various SPD processes [34], [55]. In addition to these two properties, the electrical conductivity also matches well with prior literature [[99]]. The lower electrical conductivity for the higher strained sample, despite having a comparable grain size to the lower strained material (378 ± 53 nm vs. 313 ± 30 nm, respectively) is indicative of the increasing dislocation density with straining common in SPD [2]. Compared to other HPS works, the results presented here also agree well with regards to achieving homogeneity throughout the processed sample. Thus, it is reasonable to infer that upscaled HPS [100] or HPS with incremental feeding [101] can be applied to pure copper to make homogeneous sheets. For other modified varieties of HPS, such as multi-pass HPS [102] and those that can make pipes [103] and rods [104], prior works have shown that a greater

amount of strain is necessary to achieve homogeneity. Therefore, the strain-driven grain growth apparent at higher strains for copper may also be present after these processes.

The appearance of the wavy, uneven nanocrystalline region immediately below the wear surface, referred to as the nanostructured mixing layer (NML), agrees with prior reports for low-speed sliding wear [46], [47]. It is surprising that the perpendicular test saw lower grain coarsening in the region below this NML. Prior work has instead found a correlation whereby wear rate increases with dynamically recrystallized grain size below the NML [47]. The lower normal force used for the wear tests in the current study may have contributed to this difference, as these prior works used higher loads and thus a higher stress state that may have increased flow stress. Additionally, it is possible that the deformation for the parallel wear test contributed less toward material removal and more toward dynamic recrystallization of the microstructure below the track, and vice versa for the higher wear rate perpendicular test.

Altogether, the measured properties for copper processed by HPS has not shown significant deviations from expectations based on prior SPD literature.

Wear results validate relationship between strain path and wear path

The present results are in agreement with our prior study of wear in HPT where wear rate was seen to increase when tested perpendicular to the shear path [84]. In the author's prior work, the circumferential shearing made for a slightly different wear path relationship than the more idealized fully perpendicular vs. fully parallel testing in the present work. The

prior “radial” wear tests on HPT copper were perpendicular to the shearing along the entire track, while the “tangential” tests were parallel to the shearing only at the center of the wear tracks. Depending on the radial distance of the test, both ends of the “tangential” wear tracks were either less parallel (near center) or more parallel (near edge) to the shear path. Thus, the observation of a slight decrease in wear rate for the three “tangential” wear tracks in the highly strained HPT disc in Figure 4.2 work may be considered as a reflection of the tests becoming increasingly parallel to the shear direction, further solidifying the hypothesized relationship between wear path and strain path.

While wear anisotropy in SPD materials has been underreported, a mechanistic explanation for this behavior can be assembled from various reports in the literature on deformation behaviors. In ECAE for different processing routes, anisotropy in the Bauschinger effect was seen when testing cyclic tension and compression on different orientations of samples in relation to the processing shear [105]. All ECAE processing routes showed the lowest influence of the Bauschinger effect when the samples were oriented parallel to the extrusion direction, analogous to the orientation of our parallel wear tests in HPS strips. For ECAE route A, which is most comparable to the HPS in our study, the highest resolved shear stress was found in tests oriented similarly to our perpendicular wear tests indicating slip is most likely to occur due to this orientation. In the current reciprocating wear tests, the Bauschinger effect arises since the microstructure is continually subjected to alternating tensile and compressive stresses as the wear ball scrapes back and forth across the surface. Haouaoui et al. noted that texture and grain refinement alone could not account for the observed behaviors and theorized that grain morphology and grain boundary character play

a large role. Simulation of plowing on nanocrystalline copper has shown that bulging ahead of the plow, a precursor to wear and material removal, is dependent on crystallographic orientation as well [106]. For elongated SPD grains at low strains, as in this work, a predominant C component to texture was seen for pure copper, whereas equiaxed grains were oriented in normal shear textures [107]. Another work saw shear components for the texture of copper processed by HPT under various strains [108]. It has been determined that in moderately textured copper, significant anisotropy in elastic modulus can be observed [109]. Such stiffness anisotropy may contribute to differences in deformation which lead to the different rates of material removal that underpin the observed wear results.

Reexamining the literature, more wear studies that further reinforce the relationship between wear rate and processing direction can be identified. Work on rolled aluminum [68] and steel [71] saw higher wear rates when reciprocating sliding was conducted parallel to the rolling direction. Due to symmetry, there exists a 90° relationship between the orientation of rolling texture and shear texture for FCC metals [110], so it is conceivable that these rolling studies found relationships that were orthogonal to the current study. In a Al_3Ti alloy processed by two routes of ECAE, conflicting anisotropy in wear behavior was observed [111]. A slight increase in wear rate was seen for parallel tests via route A, while a stronger decrease was seen for parallel tests in route B_c. Alternatively, prior anisotropic wear behavior was noted for a magnesium alloy with an HCP crystal structure [112]. Unlike our FCC copper, magnesium has much stronger crystallographic anisotropy.

Wear rates were also observed to be different for the two sliding directions even for the unprocessed baseline Cu sample. While not evident from any morphological anisotropy in the grain structure (Fig. 1b), the initial plate may have been supplied in the as-rolled condition, thereby containing a preferential strong rolling texture, that would be superimposed on by the HPS processing. This further highlights the utility of comparing wear results with normalized wear rates, which helped cancel out the influence of certain wear test parameters to isolate the influence of the processing changes on wear behavior. It is the hope of the authors that future works will increasingly utilize normalized wear rates for comparison across different studies.

While this work dealt with dry sliding of copper, future work can determine if the same behavior is encountered under lubricated conditions or in other material systems. At present, it is conjectured that texture from processing will not only affect wear via different mechanical properties, but also different surface wetting and oxidation behavior. Thus, it is possible that these mechanisms may dominate such that a different relationship between wear and processing direction arise for lubricated conditions.

Conclusions

Wear testing at different orientations in relation to HPS processing indicates that wear resistance in pure copper is stronger for dry sliding along a direction parallel to the shearing direction. This relationship agrees with numerous prior works. Mechanistic justifications for this behavior are found in relation to the existence of anisotropy for the Bauschinger

effect, which may be related to crystallographic texture or other microstructural features. Furthermore, it has been shown that pure copper processed by HPS exhibits expected values for average grain size, microhardness, electrical conductivity, and wear rate compared to similar straining from other SPD processes. Finally, researchers should be aware of the directional dependence between wear and strain when conducting wear studies and comparing across the literature.

Acknowledgements

HPT was carried out in the International Research Center on Giant Straining for Advanced Materials (IRC-GSAM) at Kyushu University, Japan. EHR was supported by the GAANN Fellowship from the Department of Education through the Mechanical Engineering Department at the University of California, Riverside. SNM was supported via NSF CMMI Grant #1663522.

Conclusions

In these studies, property variations with strain have been correlated between different SPD processes for pure copper. After HPT, variations in wear behavior and electrical conductivity with processing strain have been illuminated through novel data analysis and testing methods. By using precise strain-based characterization, wear and conductivity were shown to vary according to similar trends as hardness and microstructural evolution across equivalent strains. An equivalent strain between 15 and 25, previously shown to be sufficient for microstructural and hardness saturation in the wider SPD literature, was sufficient for saturation in wear resistance and electrical conductivity in the studies presented here. Furthermore, these studies have highlighted a few works in the literature that prove to be exceptions to the trends. In the case of the wear studies, these exceptions typically indicated certain confounding factors in the processing methods that complicated a simple comparison of equivalent strains. In the electrical conductivity study, the deviation from one work indicated that their testing methods inadequately accounted for error and variability. Awareness of relationships between certain properties with strain can thus help reconcile conflicting reports from the literature.

The strain-based conductivity and wear measurements also illuminated some trends with strain that had previously gone undetected. Past the strain necessary for microhardness saturation, there was a slight increase in conductivity with strain, as corroborated by a prior report. This could be explained by strain causing rearrangement of dislocation structures toward more conductive pathways. Thus, there may be some benefit to straining past

saturation, although the limits of this increase in conductivity remains to be seen. The strain-based wear testing in HPT copper indicated a potential relationship between wear path and strain path. Wear rates were higher when measured perpendicular to the rotational applied shear as compared to measurements more parallel to this shearing, despite having the same average strain and all other test parameters being identical.

To explore the directional dependence between wear and strain, wear testing was conducted on copper processed by HPS both parallel and perpendicular to the processing direction. Characterization after HPS processing revealed similar structural evolution compared to prior SPD literature. The HPS wear testing also showed variation in wear resistance when sliding in different directions with respect to the processing strain. Other SPD works in the literature also indicated a relationship whereby wear resistance is higher when measured parallel to the applied processing shear. Since reciprocating sliding wear creates alternating strain fields below the worn surface, previously reported anisotropy of the Bauschinger effect can explain the directional dependence of wear. Also contributing to this directional wear relationship is anisotropy in elastic modulus which relates to the texture and grain evolution in SPD materials. Thus, researchers should be aware of the directional dependence of wear measurements, and take this into account when planning or conducting wear tests and when comparing with other works in the literature.

Altogether, the novel strain-based characterization and analysis used in the present studies enabled the ability to observe the relationship with strain for conductivity and wear, demonstrating the power of this investigative framework for property exploration. Future studies should replicate the strain-based testing and literature comparison conducted herein

to explore variation in other properties, for example magnetic properties or antibacterial resistance. Such exploration could be informative for advancing materials development to address current problems in energy, public health, and beyond.

References

[1] V. Segal, “Review: Modes and Processes of Severe Plastic Deformation (SPD),” *Materials*, vol. 11, p. 1175, Jul. 2018, doi: 10.3390/ma11071175.

[2] Y. Cao, S. Ni, X. Liao, M. Song, and Y. Zhu, “Structural evolutions of metallic materials processed by severe plastic deformation,” *Mater. Sci. Eng. R Rep.*, vol. 133, pp. 1–59, Nov. 2018, doi: 10.1016/j.mser.2018.06.001.

[3] Y. Harai, Y. Ito, and Z. Horita, “High-pressure torsion using ring specimens,” *Scr. Mater.*, vol. 58, no. 6, pp. 469–472, Mar. 2008, doi: 10.1016/j.scriptamat.2007.10.037.

[4] G. Sakai, K. Nakamura, Z. Horita, and T. G. Langdon, “Developing high-pressure torsion for use with bulk samples,” *Mater. Sci. Eng. A*, vol. 406, no. 1, pp. 268–273, Oct. 2005, doi: 10.1016/j.msea.2005.06.049.

[5] K. Edalati and Z. Horita, “Continuous high-pressure torsion,” *J. Mater. Sci.*, vol. 45, no. 17, pp. 4578–4582, Sep. 2010, doi: 10.1007/s10853-010-4381-z.

[6] Y. Ivanisenko, A. Kilmametov, H. Rösner, and R. Z. Valiev, “Evidence of $\alpha \rightarrow \omega$ phase transition in titanium after high pressure torsion,” *Int. J. Mater. Res.*, vol. 99, no. 1, pp. 36–41, Jan. 2008, doi: 10.3139/146.101606.

[7] B. Ahn, A. P. Zhilyaev, H.-J. Lee, M. Kawasaki, and T. G. Langdon, “Rapid synthesis of an extra hard metal matrix nanocomposite at ambient temperature,” *Mater. Sci. Eng. A*, vol. 635, pp. 109–117, May 2015, doi: 10.1016/j.msea.2015.03.042.

[8] Z. Horita, Y. Tang, T. Masuda, and Y. Takizawa, “Severe Plastic Deformation under High Pressure: Upsizing Sample Dimensions,” *Mater. Trans.*, vol. 61, no. 7, pp. 1177–1190, 2020, doi: 10.2320/matertrans.MT-M2020074.

[9] V. Segal, “Equal-Channel Angular Extrusion (ECAE): From a Laboratory Curiosity to an Industrial Technology,” *Metals*, vol. 10, no. 2, Art. no. 2, Feb. 2020, doi: 10.3390/met10020244.

[10] A. Azushima *et al.*, “Severe plastic deformation (SPD) processes for metals,” *CIRP Ann.*, vol. 57, no. 2, pp. 716–735, Jan. 2008, doi: 10.1016/j.cirp.2008.09.005.

[11] Z. C. Cordero, B. E. Knight, and C. A. Schuh, “Six decades of the Hall–Petch effect – a survey of grain-size strengthening studies on pure metals,” *Int. Mater. Rev.*, vol. 61, no. 8, pp. 495–512, Nov. 2016, doi: 10.1080/09506608.2016.1191808.

[12] N. Gao, C. T. Wang, R. J. K. Wood, and T. G. Langdon, “Tribological properties of ultrafine-grained materials processed by severe plastic deformation,” *J. Mater. Sci.*, vol. 47, no. 12, pp. 4779–4797, Jun. 2012, doi: 10.1007/s10853-011-6231-z.

[13] V. Parmar *et al.*, “Relationship between Dislocation Density and Antibacterial Activity of Cryo-Rolled and Cold-Rolled Copper,” *Mater. Basel Switz.*, vol. 12, no. 2, Jan. 2019, doi: 10.3390/ma12020200.

[14] S. K and C. V, “Effectiveness of Nanomaterial Copper Cold Spray Surfaces on Inactivation of Influenza A Virus,” *J. Biotechnol. Biomater.*, vol. 05, no. 04, 2015, doi: 10.4172/2155-952X.1000205.

[15] R. Z. Valiev, Y. Estrin, Z. Horita, T. G. Langdon, M. J. Zechetbauer, and Y. T. Zhu, “Producing bulk ultrafine-grained materials by severe plastic deformation,” *JOM*, vol. 58, no. 4, pp. 33–39, Apr. 2006, doi: 10.1007/s11837-006-0213-7.

[16] K. Edalati and Z. Horita, “High-pressure torsion of pure metals: Influence of atomic bond parameters and stacking fault energy on grain size and correlation with hardness,” *Acta Mater.*, vol. 59, no. 17, pp. 6831–6836, Oct. 2011, doi: 10.1016/j.actamat.2011.07.046.

[17] K. Edalati, M. Ashida, Z. Horita, T. Matsui, and H. Kato, “Wear resistance and tribological features of pure aluminum and Al–Al2O3 composites consolidated by high-pressure torsion,” *Wear*, vol. 310, no. 1, pp. 83–89, Feb. 2014, doi: 10.1016/j.wear.2013.12.022.

[18] H. Kato, Y. Todaka, M. Umemoto, K. Morisako, M. Hashimoto, and M. Haga, “Dry Sliding Wear Properties of Sub-Microcrystalline Ultra-Low Carbon Steel Produced by High-Pressure Torsion Straining,” *Mater. Trans.*, vol. 53, no. 1, pp. 128–132, Jan. 2012, doi: 10.2320/matertrans.MD201118.

[19] H. Kato, Y. Todaka, M. Umemoto, M. Haga, and E. Sentoku, “Sliding wear behavior of sub-microcrystalline pure iron produced by high-pressure torsion straining,” *Wear*, vol. 336–337, pp. 58–68, Aug. 2015, doi: 10.1016/j.wear.2015.04.014.

[20] G. Purcek, H. Yanar, M. Demirtas, D. V. Shangina, N. R. Bochvar, and S. V. Dobatkin, “Microstructural, mechanical and tribological properties of ultrafine-grained Cu–Cr–Zr alloy processed by high pressure torsion,” *J. Alloys Compd.*, vol. 816, p. 152675, Mar. 2020, doi: 10.1016/j.jallcom.2019.152675.

[21] A. P. Zhilyaev, I. Shakhova, A. Belyakov, R. Kaibyshev, and T. G. Langdon, "Wear resistance and electroconductivity in copper processed by severe plastic deformation," *Wear*, vol. 305, no. 1, pp. 89–99, Jul. 2013, doi: 10.1016/j.wear.2013.06.001.

[22] S.-H. Joo, D.-H. Pi, J. Guo, H. Kato, S. Lee, and H. S. Kim, "Enhanced wear resistivity of a Zr-based bulk metallic glass processed by high-pressure torsion under reciprocating dry conditions," *Met. Mater. Int.*, vol. 22, no. 3, pp. 383–390, May 2016, doi: 10.1007/s12540-016-5331-3.

[23] J.-K. Han, H.-J. Lee, J. Jang, M. Kawasaki, and T. G. Langdon, "Micro-mechanical and tribological properties of aluminum-magnesium nanocomposites processed by high-pressure torsion," *Mater. Sci. Eng. A*, vol. 684, pp. 318–327, Jan. 2017, doi: 10.1016/j.msea.2016.12.067.

[24] M. I. A. E. Aal and H. S. Kim, "Wear properties of high pressure torsion processed ultrafine grained Al–7%Si alloy," *Mater. Des.*, vol. 53, pp. 373–382, Jan. 2014, doi: 10.1016/j.matdes.2013.07.045.

[25] P. Seenuvasaperumal, K. Doi, D. A. Basha, A. Singh, A. Elayaperumal, and K. Tsuchiya, "Wear behavior of HPT processed UFG AZ31B magnesium alloy," *Mater. Lett.*, vol. 227, pp. 194–198, Sep. 2018, doi: 10.1016/j.matlet.2018.05.076.

[26] M. I. Abd El Aal, "Wear properties of copper and copper composites powders consolidated by high-pressure torsion," *Friction*, vol. 8, no. 2, pp. 433–450, Apr. 2020, doi: 10.1007/s40544-019-0285-3.

[27] S. Faghihi, D. Li, and J. A. Szpunar, "Tribocorrosion behaviour of nanostructured titanium substrates processed by high-pressure torsion," *Nanotechnology*, vol. 21, no. 48, p. 485703, Nov. 2010, doi: 10.1088/0957-4484/21/48/485703.

[28] C. Gode, H. Yilmazer, I. Ozdemir, and Y. Todaka, "Microstructural refinement and wear property of Al–Si–Cu composite subjected to extrusion and high-pressure torsion," *Mater. Sci. Eng. A*, vol. 618, pp. 377–384, Nov. 2014, doi: 10.1016/j.msea.2014.09.011.

[29] G. Purcek, H. Yanar, D. V. Shangina, M. Demirtas, N. R. Bochvar, and S. V. Dobatkin, "Influence of high pressure torsion-induced grain refinement and subsequent aging on tribological properties of Cu-Cr-Zr alloy," *J. Alloys Compd.*, vol. 742, pp. 325–333, Apr. 2018, doi: 10.1016/j.jallcom.2018.01.303.

[30] J.-K. Han, D. K. Han, G. Y. Liang, J.-I. Jang, T. G. Langdon, and M. Kawasaki, "Direct Bonding of Aluminum–Copper Metals through High-Pressure Torsion Processing," *Adv. Eng. Mater.*, vol. 20, no. 11, p. 1800642, 2018, doi: https://doi.org/10.1002/adem.201800642.

[31] S. Shahrezaei, Y. Sun, and S. N. Mathaudhu, “Strength-ductility modulation via surface severe plastic deformation and annealing,” *Mater. Sci. Eng. A*, vol. 761, p. 138023, Jul. 2019, doi: 10.1016/j.msea.2019.06.033.

[32] Z. Horita and T. G. Langdon, “Microstructures and microhardness of an aluminum alloy and pure copper after processing by high-pressure torsion,” *Mater. Sci. Eng. A*, vol. 410–411, pp. 422–425, Nov. 2005, doi: 10.1016/j.msea.2005.08.133.

[33] J. Li, J. Xu, C. T. Wang, D. Shan, B. Guo, and T. G. Langdon, “Microstructural Evolution and Micro-Compression in High-Purity Copper Processed by High-Pressure Torsion,” *Adv. Eng. Mater.*, vol. 18, no. 2, pp. 241–250, Feb. 2016, doi: 10.1002/adem.201500488.

[34] T. Hebesberger, H. P. Stüwe, A. Vorhauer, F. Wetscher, and R. Pippan, “Structure of Cu deformed by high pressure torsion,” *Acta Mater.*, vol. 53, no. 2, pp. 393–402, Jan. 2005, doi: 10.1016/j.actamat.2004.09.043.

[35] K. Edalati, T. Fujioka, and Z. Horita, “Microstructure and mechanical properties of pure Cu processed by high-pressure torsion,” *Mater. Sci. Eng. A*, vol. 497, no. 1, pp. 168–173, Dec. 2008, doi: 10.1016/j.msea.2008.06.039.

[36] F. Wetscher, A. Vorhauer, and R. Pippan, “Strain hardening during high pressure torsion deformation,” *Mater. Sci. Eng. A*, vol. 410–411, pp. 213–216, Nov. 2005, doi: 10.1016/j.msea.2005.08.027.

[37] J. F. Archard, “Contact and Rubbing of Flat Surfaces,” *J. Appl. Phys.*, vol. 24, no. 8, pp. 981–988, Aug. 1953, doi: 10.1063/1.1721448.

[38] T. Miyajima and Y. Iwai, “Effects of reinforcements on sliding wear behavior of aluminum matrix composites,” *Wear*, vol. 255, no. 1, pp. 606–616, Aug. 2003, doi: 10.1016/S0043-1648(03)00066-8.

[39] Z. Han, L. Lu, and K. Lu, “Dry sliding tribological behavior of nanocrystalline and conventional polycrystalline copper,” *Tribol. Lett.*, vol. 21, no. 1, pp. 45–50, Jan. 2006, doi: 10.1007/s11249-005-9007-2.

[40] X. Chen, Z. Han, and K. Lu, “Friction and Wear Reduction in Copper with a Gradient Nano-grained Surface Layer,” *ACS Appl. Mater. Interfaces*, vol. 10, no. 16, pp. 13829–13838, Apr. 2018, doi: 10.1021/acsami.8b01205.

[41] Y. S. Li, N. R. Tao, and K. Lu, “Microstructural evolution and nanostructure formation in copper during dynamic plastic deformation at cryogenic temperatures,” *Acta Mater.*, vol. 56, no. 2, pp. 230–241, Jan. 2008, doi: 10.1016/j.actamat.2007.09.020.

[42] W. L. Li, N. R. Tao, Z. Han, and K. Lu, “Comparisons of dry sliding tribological behaviors between coarse-grained and nanocrystalline copper,” *Wear*, vol. 274–275, pp. 306–312, Jan. 2012, doi: 10.1016/j.wear.2011.09.010.

[43] Y. S. Zhang, Z. Han, K. Wang, and K. Lu, “Friction and wear behaviors of nanocrystalline surface layer of pure copper,” *Wear*, vol. 260, no. 9, pp. 942–948, May 2006, doi: 10.1016/j.wear.2005.06.010.

[44] J. Moering *et al.*, “The role of shear strain on texture and microstructural gradients in low carbon steel processed by Surface Mechanical Attrition Treatment,” *Scr. Mater.*, vol. 108, pp. 100–103, Nov. 2015, doi: 10.1016/j.scriptamat.2015.06.027.

[45] C. Greiner, Z. Liu, L. Strassberger, and P. Gumbsch, “Sequence of Stages in the Microstructure Evolution in Copper under Mild Reciprocating Tribological Loading,” *ACS Appl. Mater. Interfaces*, vol. 8, no. 24, pp. 15809–15819, Jun. 2016, doi: 10.1021/acsami.6b04035.

[46] A. Emge, S. Karthikeyan, and D. A. Rigney, “The effects of sliding velocity and sliding time on nanocrystalline tribolayer development and properties in copper,” *Wear*, vol. 267, no. 1, pp. 562–567, Jun. 2009, doi: 10.1016/j.wear.2008.12.102.

[47] B. Yao, Z. Han, and K. Lu, “Correlation between wear resistance and subsurface recrystallization structure in copper,” *Wear*, vol. 294–295, pp. 438–445, Jul. 2012, doi: 10.1016/j.wear.2012.07.008.

[48] R. Pippan, S. Scheriau, A. Taylor, M. Hafok, A. Hohenwarter, and A. Bachmaier, “Saturation of Fragmentation During Severe Plastic Deformation,” *Annu. Rev. Mater. Res.*, vol. 40, no. 1, pp. 319–343, Jun. 2010, doi: 10.1146/annurev-matsci-070909-104445.

[49] S. Erbel, “Mechanical properties and structure of extremely strainhardened copper,” *Met. Technol.*, vol. 6, no. 1, pp. 482–486, Jan. 1979, doi: 10.1179/030716979803276363.

[50] X. H. An, S. D. Wu, Z. F. Zhang, R. B. Figueiredo, N. Gao, and T. G. Langdon, “Evolution of microstructural homogeneity in copper processed by high-pressure torsion,” *Scr. Mater.*, vol. 63, no. 5, pp. 560–563, Sep. 2010, doi: 10.1016/j.scriptamat.2010.05.030.

[51] A. I. Almazrouee, K. J. Al-Fadhalah, S. N. Alhajeri, and T. G. Langdon, “Microstructure and microhardness of OFHC copper processed by high-pressure torsion,” *Mater. Sci. Eng. A*, vol. 641, pp. 21–28, Aug. 2015, doi: 10.1016/j.msea.2015.06.016.

[52] J. Čížek *et al.*, “Evolution of defects in copper deformed by high-pressure torsion,” *Acta Mater.*, vol. 59, no. 6, pp. 2322–2329, Apr. 2011, doi: 10.1016/j.actamat.2010.12.028.

[53] D. J. Lee *et al.*, “Dislocation density-based finite element analysis of large strain deformation behavior of copper under high-pressure torsion,” *Acta Mater.*, vol. 76, pp. 281–293, Sep. 2014, doi: 10.1016/j.actamat.2014.05.027.

[54] Y. Huang, S. Sabbaghianrad, A. I. Almazrouee, K. J. Al-Fadhalah, S. N. Alhajeri, and T. G. Langdon, “The significance of self-annealing at room temperature in high purity copper processed by high-pressure torsion,” *Mater. Sci. Eng. A*, vol. 656, pp. 55–66, Feb. 2016, doi: 10.1016/j.msea.2016.01.027.

[55] K. Edalati, K. Imamura, T. Kiss, and Z. Horita, “Equal-Channel Angular Pressing and High-Pressure Torsion of Pure Copper: Evolution of Electrical Conductivity and Hardness with Strain,” *Mater. Trans.*, vol. 53, no. 1, pp. 123–127, 2012, doi: 10.2320/matertrans.MD201109.

[56] J. C. Springs, Y. T. Kao, A. Srivastava, Z. S. Levin, R. E. Barber, and K. T. Hartwig, “Strength and electrical resistivity of heavily worked copper,” *IOP Conf. Ser. Mater. Sci. Eng.*, vol. 279, no. 1, p. 012003, 2017, doi: 10.1088/1757-899X/279/1/012003.

[57] R. Jamaati and M. R. Toroghinejad, “Application of ARB process for manufacturing high-strength, finely dispersed and highly uniform Cu/Al2O3 composite,” *Mater. Sci. Eng. A*, vol. 527, no. 27, pp. 7430–7435, Oct. 2010, doi: 10.1016/j.msea.2010.08.038.

[58] A. I. Almazrouee, K. J. Al-Fadhalah, S. N. Alhajeri, Y. Huang, and T. G. Langdon, “Effect of Long-Term Storage on Microstructure and Microhardness Stability in OFHC Copper Processed by High-Pressure Torsion,” *Adv. Eng. Mater.*, vol. 21, no. 5, p. 1801300, 2019, doi: https://doi.org/10.1002/adem.201801300.

[59] A. V. Filippov, S. Yu. Tarasov, S. V. Fortuna, O. A. Podgornykh, N. N. Shamarin, and A. V. Vorontsov, “Wear, vibration and acoustic emission characterization of sliding friction processes of coarse-grained and ultrafine-grained copper,” *Wear*, vol. 424–425, pp. 78–88, Apr. 2019, doi: 10.1016/j.wear.2019.02.014.

[60] A. P. Zhilyaev, A. Morozova, J. M. Cabrera, R. Kaibyshev, and T. G. Langdon, “Wear resistance and electroconductivity in a Cu–0.3Cr–0.5Zr alloy processed by ECAP,” *J. Mater. Sci.*, vol. 52, no. 1, pp. 305–313, Jan. 2017, doi: 10.1007/s10853-016-0331-8.

[61] P. Iglesias, M. D. Bermúdez, W. Moscoso, and S. Chandrasekar, “Influence of processing parameters on wear resistance of nanostructured OFHC copper manufactured by large strain extrusion machining,” *Wear*, vol. 268, no. 1, pp. 178–184, Jan. 2010, doi: 10.1016/j.wear.2009.07.009.

[62] T. L. Brown *et al.*, “A study of the interactive effects of strain, strain rate and temperature in severe plastic deformation of copper,” *Acta Mater.*, vol. 57, no. 18, pp. 5491–5500, Oct. 2009, doi: 10.1016/j.actamat.2009.07.052.

[63] T. J. Rupert and C. A. Schuh, “Sliding wear of nanocrystalline Ni–W: Structural evolution and the apparent breakdown of Archard scaling,” *Acta Mater.*, vol. 58, no. 12, pp. 4137–4148, Jul. 2010, doi: 10.1016/j.actamat.2010.04.005.

[64] D. Odabaş and Ş. Su, “A comparison of the reciprocating and continuous two-body abrasive wear behavior of solution-treated and age-hardened 2014 Al alloy,” *Wear*, vol. 208, no. 1, pp. 25–35, Jul. 1997, doi: 10.1016/S0043-1648(96)07378-4.

[65] C. Tang, J. M. Wang, G. W. Wen, Y. Wang, and D. Y. Li, “Bauschinger effect in wear of Cu–40Zn alloy and its variations with the wear condition,” *Wear*, vol. 271, no. 9, pp. 1237–1243, Jul. 2011, doi: 10.1016/j.wear.2010.11.026.

[66] M. Ruiz-Andres, A. Conde, J. De Damborenea, and I. Garcia, “Influence of sliding direction changes, contact frequency and Bauschinger effect on the wear of dual phase steels,” *Tribol. Int.*, vol. 92, pp. 485–492, Dec. 2015, doi: 10.1016/j.triboint.2015.07.033.

[67] L. Yue, H. Zhang, and D. Y. Li, “Defect generation in nano-twinned, nano-grained and single crystal Cu systems caused by wear: A molecular dynamics study,” *Scr. Mater.*, vol. 63, no. 11, pp. 1116–1119, Nov. 2010, doi: 10.1016/j.scriptamat.2010.08.019.

[68] D. H. Buckley, *The Effect of Orientation and the Presence of Surface Active Materials on the Friction, Deformation and Wear of Aluminum*. National Aeronautics and Space Administration, 1969.

[69] F. A. Sadykov, N. P. Barykin, and I. R. Aslanyan, “Wear of copper and its alloys with submicrocrystalline structure,” *Wear*, vol. 225–229, pp. 649–655, Apr. 1999, doi: 10.1016/S0043-1648(98)00374-3.

[70] H. Sato, S. El Hadad, O. Sitdikov, and Y. Watanabe, “Effects of Processing Routes on Wear Property of Al-Al3Ti Alloys Severely Deformed by ECAP,” *Materials Science Forum*, 2008. https://www.scientific.net/MSF.584-586.971 (accessed Dec. 13, 2019).

[71] H. Krause and E. Öcalan, “The effect of initial orientation on the formation of tribological textures and on the wear behaviour of the region in the proximity of surface layers under continuous sliding motion in tribological systems,” *Wear*, vol. 108, no. 4, pp. 337–343, Apr. 1986, doi: 10.1016/0043-1648(86)90011-6.

[72] S. Yu. Tarasov, D. V. Lychagin, and A. V. Chumaevskii, “Orientation dependence of subsurface deformation in dry sliding wear of Cu single crystals,” *Appl. Surf. Sci.*, vol. 274, pp. 22–26, Jun. 2013, doi: 10.1016/j.apsusc.2013.02.018.

[73] W. Cai, P. Bellon, and A. J. Beaudoin, “Probing the subsurface lattice rotation dynamics in bronze after sliding wear,” *Scr. Mater.*, vol. 172, pp. 6–11, Nov. 2019, doi: 10.1016/j.scriptamat.2019.07.002.

[74] A. Mahato, N. K. Sundaram, H. Yeung, M. Lukitsch, A. K. Sachdev, and S. Chandrasekar, “Quantitative In Situ Analysis of Deformation in Sliding Metals: Effect of Initial Strain State,” *Tribol. Lett.*, vol. 60, no. 3, p. 36, Oct. 2015, doi: 10.1007/s11249-015-0612-4.

[75] N. Beckmann *et al.*, “Origins of Folding Instabilities on Polycrystalline Metal Surfaces,” *Phys. Rev. Appl.*, vol. 2, no. 6, p. 064004, Dec. 2014, doi: 10.1103/PhysRevApplied.2.064004.

[76] S. Becker, K. Schulz, D. Scherhaufer, P. Gumbsch, and C. Greiner, “Variations in strain affect friction and microstructure evolution in copper under a reciprocating tribological load,” *J. Mater. Res.*, Jan. 2021, doi: 10.1557/s43578-020-00050-z.

[77] G. Rogl *et al.*, “Influence of shear strain on HPT-processed n-type skutterudites yielding ZT=2.1,” *J. Alloys Compd.*, vol. 855, p. 157409, Feb. 2021, doi: 10.1016/j.jallcom.2020.157409.

[78] A. Rijal, S. P. Singh, J.-K. Han, M. Kawasaki, and P. Kumar, “Effect of High-Pressure Torsion on Hardness and Electrical Resistivity of Commercially Pure Cu,” *Adv. Eng. Mater.*, vol. 22, no. 1, p. 1900547, 2020, doi: https://doi.org/10.1002/adem.201900547.

[79] J. M. Cubero-Sesin, H. In, M. Arita, H. Iwaoka, and Z. Horita, “High-pressure torsion for fabrication of high-strength and high-electrical conductivity Al micro-wires,” *J. Mater. Sci.*, vol. 49, no. 19, pp. 6550–6557, Oct. 2014, doi: 10.1007/s10853-014-8240-1.

[80] R. Haraguchi, Y. Yoshimatsu, T. Nagaoka, M. Arita, K. Edalati, and Z. Horita, “Electrical resistivity mapping of titanium and zirconium discs processed by high-pressure torsion for homogeneity and phase transformation evaluation,” *J. Mater. Sci.*, vol. 52, no. 11, pp. 6778–6788, Jun. 2017, doi: 10.1007/s10853-017-0916-x.

[81] Y. Huang *et al.*, "The fabrication of graphene-reinforced Al-based nanocomposites using high-pressure torsion," *Acta Mater.*, vol. 164, pp. 499–511, Feb. 2019, doi: 10.1016/j.actamat.2018.10.060.

[82] R. K. Islamgaliev, K. M. Nesterov, J. Bourgon, Y. Champion, and R. Z. Valiev, "Nanostructured Cu-Cr alloy with high strength and electrical conductivity," *J. Appl. Phys.*, vol. 115, no. 19, p. 194301, May 2014, doi: 10.1063/1.4874655.

[83] M. Ashida, T. Hamachiyo, K. Hasezaki, H. Matsunoshita, M. Kai, and Z. Horita, "Texture of bismuth telluride-based thermoelectric semiconductors processed by high-pressure torsion," *J. Phys. Chem. Solids*, vol. 70, no. 7, pp. 1089–1092, Jul. 2009, doi: 10.1016/j.jpcs.2009.06.002.

[84] E. Ramos, T. Masuda, S. Shahrezaei, Z. Horita, and S. Mathaudhu, "Strain effects on the wear rate of severely deformed copper," *ArXiv210909907 Cond-Mat Phys.*, Sep. 2021, Accessed: Oct. 07, 2021. [Online]. Available: http://arxiv.org/abs/2109.09907

[85] D. Waryoba, Z. Islam, B. Wang, and A. Haque, "Low temperature annealing of metals with electrical wind force effects," *J. Mater. Sci. Technol.*, vol. 35, no. 4, pp. 465–472, Apr. 2019, doi: 10.1016/j.jmst.2018.09.069.

[86] Keithley Instruments, *Low level Measurements Handbook*, 7th ed. Cleveland, OH: Keithley Instruments Inc., 2018.

[87] K. M. Mannan and K. R. Karim, "Grain boundary contribution to the electrical conductivity of polycrystalline Cu films," *J. Phys. F Met. Phys.*, vol. 5, no. 9, pp. 1687–1693, Sep. 1975, doi: 10.1088/0305-4608/5/9/009.

[88] N. Takata, S.-H. Lee, and N. Tsuji, "Ultrafine grained copper alloy sheets having both high strength and high electric conductivity," *Mater. Lett.*, vol. 63, no. 21, pp. 1757–1760, Aug. 2009, doi: 10.1016/j.matlet.2009.05.021.

[89] D. A. Rigney, L. H. Chen, M. G. S. Naylor, and A. R. Rosenfield, "Wear processes in sliding systems," *Wear*, vol. 100, no. 1, pp. 195–219, Dec. 1984, doi: 10.1016/0043-1648(84)90013-9.

[90] D. A. Rigney, "Large strains associated with sliding contact of metals," *Mater. Res. Innov.*, vol. 1, no. 4, pp. 231–234, Mar. 1998, doi: 10.1007/s100190050046.

[91] P. La *et al.*, "Dry-sliding tribological properties of ultrafine-grained Ti prepared by severe plastic deformation," *Acta Mater.*, vol. 53, no. 19, pp. 5167–5173, Nov. 2005, doi: 10.1016/j.actamat.2005.07.031.

[92] H. Garbacz, M. Grądzka-Dahlke, and K. J. Kurzydłowski, “The tribological properties of nano-titanium obtained by hydrostatic extrusion,” *Wear*, vol. 263, no. 1, pp. 572–578, Sep. 2007, doi: 10.1016/j.wear.2006.11.047.

[93] G. Purcek *et al.*, “Mechanical and wear properties of ultrafine-grained pure Ti produced by multi-pass equal-channel angular extrusion,” *Mater. Sci. Eng. A*, vol. 517, no. 1, pp. 97–104, Aug. 2009, doi: 10.1016/j.msea.2009.03.054.

[94] T. Fujioka and Z. Horita, “Development of High-Pressure Sliding Process for Microstructural Refinement of Rectangular Metallic Sheets,” *Mater. Trans.*, vol. 50, no. 4, pp. 930–933, 2009, doi: 10.2320/matertrans.MRP2008445.

[95] S. Ferrasse, K. T. Hartwig, R. E. Goforth, and V. M. Segal, “Microstructure and properties of copper and aluminum alloy 3003 heavily worked by equal channel angular extrusion,” *Metall. Mater. Trans. A*, vol. 28, no. 4, pp. 1047–1057, Apr. 1997, doi: 10.1007/s11661-997-0234-z.

[96] S. Özerinç, K. Tai, N. Q. Vo, P. Bellon, R. S. Averback, and W. P. King, “Grain boundary doping strengthens nanocrystalline copper alloys,” *Scr. Mater.*, vol. 67, no. 7, pp. 720–723, Oct. 2012, doi: 10.1016/j.scriptamat.2012.06.031.

[97] S. Lee, K. Tazoe, I. F. Mohamed, and Z. Horita, “Strengthening of AA7075 alloy by processing with high-pressure sliding (HPS) and subsequent aging,” *Mater. Sci. Eng. A*, vol. 628, pp. 56–61, Mar. 2015, doi: 10.1016/j.msea.2015.01.026.

[98] R. Jamaati, M. R. Toroghinejad, and H. Edris, “Effect of stacking fault energy on nanostructure formation under accumulative roll bonding (ARB) process,” *Mater. Sci. Eng. A*, vol. 578, pp. 191–196, Aug. 2013, doi: 10.1016/j.msea.2013.04.090.

[99] E. Ramos, T. Masuda, Z. Horita, and S. Mathaudhu, “Electrical conductivity characterized at varying strains in spiral cut high-pressure torsion discs.”

[100] Y. Takizawa *et al.*, “Scaling up of High-Pressure Sliding (HPS) for Grain Refinement and Superplasticity,” *Metall. Mater. Trans. A*, vol. 47, no. 9, pp. 4669–4681, Sep. 2016, doi: 10.1007/s11661-016-3623-3.

[101] Y. Takizawa *et al.*, “Incremental Feeding High-Pressure Sliding for Grain Refinement of Large-Scale Sheets: Application to Inconel 718,” *Metall. Mater. Trans. A*, vol. 49, no. 5, pp. 1830–1840, May 2018, doi: 10.1007/s11661-018-4534-2.

[102] Y. Tang, K. Sumikawa, Y. Takizawa, M. Yumoto, Y. Otagiri, and Z. Horita, “Multi-pass high-pressure sliding (MP-HPS) for grain refinement and superplasticity in metallic round rods,” *Mater. Sci. Eng. A*, vol. 748, pp. 108–118, Mar. 2019, doi: 10.1016/j.msea.2019.01.071.

[103] Y. Tang, K. Matsuda, Y. Takizawa, M. Yumoto, Y. Otagiri, and Z. Horita, "Grain refinement and superplasticity of pipes processed by high-pressure sliding," *Mater. Sci. Technol.*, vol. 36, no. 7, pp. 877–886, May 2020, doi: 10.1080/02670836.2020.1746538.

[104] T. Masuda, K. Fujimitsu, Y. Takizawa, and Z. Horita, "High-Pressure Sliding Using Rod Samples for Grain Refinement," *Lett. Mater.*, vol. 5, no. 3, pp. 258–263, Aug. 2015, doi: 10.22226/2410-3535-2015-3-258-263.

[105] M. Haouaoui, I. Karaman, and H. J. Maier, "Flow stress anisotropy and Bauschinger effect in ultrafine grained copper," *Acta Mater.*, vol. 54, no. 20, pp. 5477–5488, Dec. 2006, doi: 10.1016/j.actamat.2006.07.022.

[106] N. Beckmann *et al.*, "Origins of Folding Instabilities on Polycrystalline Metal Surfaces," *Phys. Rev. Appl.*, vol. 2, no. 6, p. 064004, Dec. 2014, doi: 10.1103/PhysRevApplied.2.064004.

[107] M. Jahedi, I. J. Beyerlein, M. H. Paydar, and M. Knezevic, "Effect of Grain Shape on Texture Formation during Severe Plastic Deformation of Pure Copper," *Adv. Eng. Mater.*, vol. 20, no. 4, p. 1600829, 2018, doi: 10.1002/adem.201600829.

[108] J. Li, J. Xu, C. T. Wang, D. Shan, B. Guo, and T. G. Langdon, "Microstructural Evolution and Micro-Compression in High-Purity Copper Processed by High-Pressure Torsion," *Adv. Eng. Mater.*, vol. 18, no. 2, pp. 241–250, Feb. 2016, doi: 10.1002/adem.201500488.

[109] S. R. Agnew and J. R. Weertman, "The influence of texture on the elastic properties of ultrafine-grain copper," *Mater. Sci. Eng. A*, vol. 242, no. 1, pp. 174–180, Feb. 1998, doi: 10.1016/S0921-5093(97)00504-2.

[110] M. Hölscher, D. Raabe, and K. Lücke, "Relationship between rolling textures and shear textures in f.c.c. and b.c.c. metals," *Acta Metall. Mater.*, vol. 42, no. 3, pp. 879–886, Mar. 1994, doi: 10.1016/0956-7151(94)90283-6.

[111] H. Sato, S. El Hadad, O. Sitdikov, and Y. Watanabe, "Effects of Processing Routes on Wear Property of Al-Al3Ti Alloys Severely Deformed by ECAP," *Mater. Sci. Forum*, vol. 584–586, pp. 971–976, 2008, doi: 10.4028/www.scientific.net/MSF.584-586.971.

[112] B. Mao, X. Zhang, P. L. Menezes, and Y. Liao, "Anisotropic microstructure evolution of an AZ31B magnesium alloy subjected to dry sliding and its effects on friction and wear performance," *Materialia*, vol. 8, p. 100444, Dec. 2019, doi: 10.1016/j.mtla.2019.100444.